

## TI Designs: TIDA-01476

# センサとクラウドとのネットワークを可能にする低消費電力、ワイヤレスPIRモーション検出器のリファレンス・デザイン



### 概要

TIDA-01476リファレンス・デザインでは、IoTネットワーク・ゲートウェイとクラウドのデータ・プロバイダに接続可能な、産業用センサ-クラウド間終端ノードを作成する方法を紹介します。このデザインは、テキサス・インスツルメンツのナノパワー・オペアンプ、コンパレータ、およびSub-1GHz SimpleLink™超低電力ワイヤレス・マイクロコントローラ (MCU) プラットフォームを使用して、バッテリー駆動時間が非常に長く、ワイヤ配線を必要としない、超低消費電力のセンサ-クラウド間のモーション検出器を実現します。

### リソース

<a href="#">TIDA-01476</a>	デザイン・フォルダ
<a href="#">LPV802</a>	プロダクト・フォルダ
<a href="#">TLV3691</a>	プロダクト・フォルダ
<a href="#">CC1310</a>	プロダクト・フォルダ



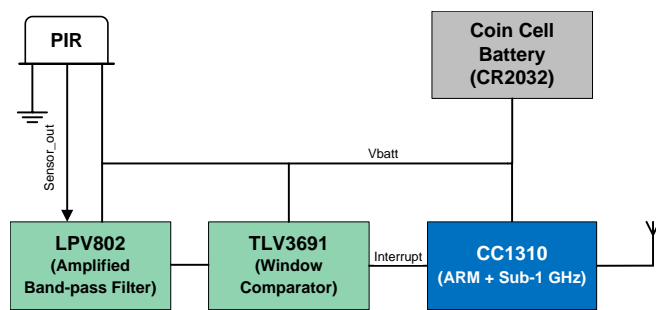
[E2Eエキスパートに質問](#)

### 特長

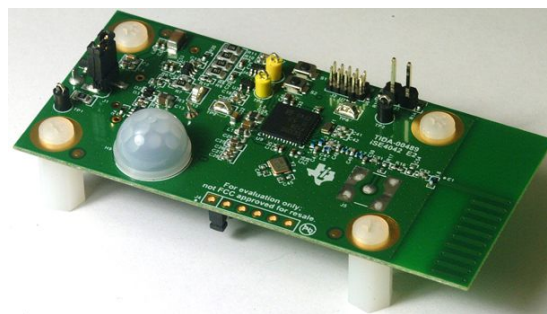
- 最大1kmの直線見通し距離を可能にする、大規模なネットワークからクラウドへの接続性
- IEEE 802.15.4e/g標準をベースとする、TI 15.4-Stack搭載のSub-1GHzソリューション
- ナノパワー・アナログを使用した超低消費電力設計により、1個のCR2032コイン電池で10年間のバッテリー駆動を実現
- 低いスタンバイ時電流: 1.65μA (スタンバイ中もPIRセンサはアクティブ)
- 割り込みを使用したSub-1GHzワイヤレス通信でのモーション通知により、さらに消費電力を低減
- 最大30フィートのモーション感度

### アプリケーション

- モーション検出
- 照明センサ
- ワイヤレス制御
- ビルディング・オートメーション



Copyright © 2016, Texas Instruments Incorporated



使用許可、知的財産、その他免責事項は、最終ページにあるIMPORTANT NOTICE(重要な注意事項)をご参照くださいますようお願いいたします。英語版のTI製品についての情報を翻訳したこの資料は、製品の概要を確認する目的で便宜的に提供しているものです。該当する正式な英語版の最新情報は、[www.ti.com](http://www.ti.com)で閲覧でき、その内容が常に優先されます。TIでは翻訳の正確性および妥当性につきましては一切保証いたしません。実際の設計などの前には、必ず最新版の英語版をご参照くださいますようお願いいたします。

## 1 System Description

Many industrial and building automation systems use motion detectors to control different functions based on human presence, such as lighting, for achieving higher efficiency of those functions by turning them off when not needed. Additionally, these systems require increasing numbers of wireless sensor nodes to reduce the installation costs and the make the systems more flexible for future expansion by eliminating wiring. However, one of the major limitations for a large wireless network is power. Because these systems are battery powered, the maintenance cost associated with periodic battery replacement can become prohibitive. Depending on the power consumption and battery configuration, typical battery-powered PIR motion detectors can run anywhere from four to seven years before the batteries need to be replaced.

Enabled by Texas Instruments' nano-power amplifiers, comparators, and the SimpleLink ultra-low-power wireless MCU platform, the Low-Power Wireless PIR Motion Detector Reference Design demonstrates a motion detector circuit solution requiring no wiring while also fully maximizing the battery life.

At a high level, this TI Design consists of a CR2032 coin cell battery, two nano-power op amps, two nano-power comparators, an ultra-low-power wireless MCU, and a PIR sensor with analog signal output. The two op amps form an amplified band-pass filter with a high-input impedance, which allows it to be connected directly to the sensor without loading it. The two comparators form a window comparator, which is used to compare the amplified sensor output to fixed reference thresholds so that motion can be distinguished from noise. The two outputs of the window comparator then serve as interrupts to the wireless MCU. This way, the MCU can operate in its lowest power sleep mode during times where there is no motion being detected and only wakes up to send messages back to a remote host when motion has been detected. Due to the nano-amp operation of the analog signal chain components, this TI Design achieves a 10-year battery life from a single CR2032 coin cell battery.

This design guide addresses component selection, design theory, software and the testing results of this TI Design system. The scope of this design guide gives system designers a head-start in integrating TI's nano-power analog components, and the SimpleLink ultra-low-power wireless MCU platform along with a starting point for sensor-to-cloud software integration.

The following subsections describe the various blocks within the TI Design system and what characteristics are most critical to best implement the corresponding function.

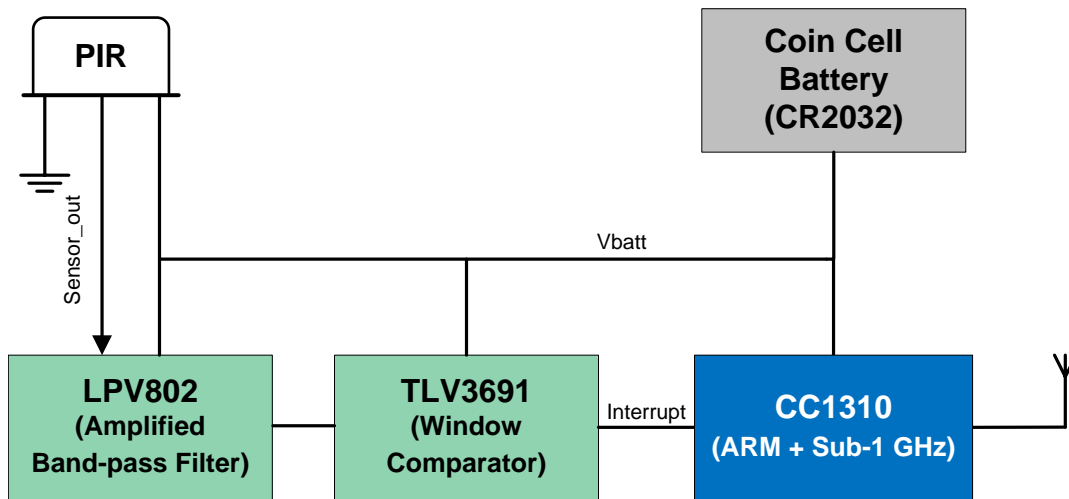
## 1.1 Key System Specifications

**表 1. Key System Specifications**

PARAMETER	SPECIFICATIONS	DETAILS
Input power source	CR2032 Lithium-ion coin cell battery (3.0-V nominal voltage)	<a href="#">2.2.4</a>
Sensor type	PIR (Pyroelectric or Passive InfraRed)	<a href="#">2.2.5</a>
Transmit-state current consumption	14 mA	<a href="#">3.2.2.1</a>
Transmit-state duration	23 ms	<a href="#">3.2.2.1</a>
Average standby-state current consumption	2.6 $\mu$ A	<a href="#">3.2.2.1</a>
Standby-state duration	1 minute of no motion detected	<a href="#">2.4.4</a>
Sleep-state current consumption	1.65 $\mu$ A	<a href="#">3.2.2.1</a>
Movements per hour assumed for lifetime calculation	6 per hour average over the battery lifetime	<a href="#">3.2.2.2</a>
Estimated battery life	10 years	<a href="#">3.2.2.2</a>
Motion sensing range	30 feet nominal	<a href="#">3.2.2.3.1</a>
Radio transmission range	> 200 meters	<a href="#">3.2.2.3.2</a>
Operating temperature	-30°C to 60°C (limited by CR2032 coin cell operating range)	<a href="#">2.2.4</a>
Operating humidity	20 to 70%	<a href="#">3.2.1.2.1</a>
Vibration	—	<a href="#">3.2.2.3.4</a>
RF immunity	30 V/m from 10 kHz to 1 GHz	<a href="#">3.2.2.3.3</a>
Working environment	Indoor and outdoor	<a href="#">2.2.4</a>
Form factor	35x75-mm rectangular PCB	<a href="#">4.3</a>

## 2 System Overview

### 2.1 Block Diagram



Copyright © 2016, Texas Instruments Incorporated

図 1. Wireless PIR System Block Diagram

## 2.2 Design Considerations

### 2.2.1 Operational Amplifiers

In this TI Design, it is necessary to amplify and filter the signal at the output of the PIR sensor so that the signal amplitudes going into following stages in the signal chain are large enough to provide useful information.

Typical signal levels at the output of a PIR sensor are in the micro-volt range for motion of distant objects, which exemplifies the need for amplification. The filtering function is necessary to primarily limit the noise bandwidth of the system before reaching the input to the window comparator. Secondly, the filtering function also serves to set limits for the minimum and maximum speed at which the system will detect movement.

For an extremely long battery life, this TI Design uses the LPV802 because of its low current consumption of 320 nA (typical) per amplifier. Other considerations that make the LPV802 ideal for this TI Design are its low input voltage offset and low input bias current, which allows use of high value resistors, and rail-to-rail operation on both input and output. Additionally, the LPV802 integrates EMI protection to reduce sensitivity to unwanted RF signals, which is useful for low-power designs because of their high-impedance nodes.

### 2.2.2 Comparators

In this TI Design, it is necessary to convert the amplified and filtered version of the sensor output into digital signals, which can be used as inputs to the MCU. To accomplish this, a window comparator circuit is used.

The low current consumption of only 75 nA (typical) per comparator makes the TLV3691 in this TI Design ideal. Other considerations for the comparator in this reference design include its low input voltage offset and low input bias current. Additionally, the TLV3691 features a rail-to-rail input stage with an input common mode range, which exceeds the supply rails by 100 mV, thereby preventing output phase inversion when the voltage at the input pins exceed the supply. This translates not only into robustness to supply noise, but also maximizes the flexibility in adjusting the window comparator thresholds in this design.

### 2.2.3 Ultra-Low-Power Wireless MCU

In this TI Design, transmitting the sensor information to some central location for processing is necessary. However, because power consumption is always a concern in battery-based applications, the radio and processor must be low power. Also, the wireless protocol required for the end-equipment system is an important consideration for the selection of the radio device.

With TI's SimpleLink ultra-low-power wireless MCU platform, low power with a combined radio and MCU enables an extremely long battery life for sensor end-nodes. Furthermore, the CC1310 is a multi-standard device with software stack support for wM-Bus and IEEE 802.15.4g. In this reference design, a TI 15.4-stack-based application handles the sensing algorithm and Sub-1 GHz communications between the gateway and the sensor node. The hardware as built can work with other protocols as well.

### 2.2.4 Coin Cell Battery

The power source for this TI Design is a CR2032 lithium-ion coin cell. The selection of the CR2032 coin cell battery as the power source was due to the ubiquity of that battery type, particularly in small form factor systems such as a sensor end-node.

The voltage characteristics of a lithium-ion CR2032 coin cell battery are also ideal. The output voltage remains relatively flat throughout the discharge life until the cell is nearly depleted. When the cell is depleted, the output voltage drops off relatively quickly.

The temperature characteristics of lithium-ion batteries are also superior to that of alkaline cells, particularly at lower temperatures. This superiority is due to lithium-ion cells having a non-aqueous electrolyte that performs better than aqueous electrolytes commonly found in alkaline batteries. However, the CR2032 coin cell battery is still the limiting component in terms of the operating temperature range; all of the integrated circuits and other electrical components are specified to operate at a wider temperature range than the battery. Therefore, the specified operating temperature range of the TI Design system is  $-30^{\circ}\text{C}$  to  $60^{\circ}\text{C}$ . Given an appropriate weather-proof enclosure, this TI Design system is suited for both indoor and outdoor use.

Immediately following the battery is a low  $R_{\text{DS\_ON}}$  P-channel MOSFET and a bulk capacitor. The P-channel MOSFET prevents damage to the hardware if the coin cell battery is inserted backwards while minimizing the forward voltage drop in normal operation. The bulk capacitor is sized to prevent too much voltage droop, particularly during the transitions into the MCU on-state for radio transmissions.

### 2.2.5 PIR Sensor

The sensor chosen for the TI Design is the Murata® IRS-B210ST01 PIR sensor. The choice of this sensor was due to the fact that it is in a surface mount package and provides an analog output so that the low-power circuit in this TI Design could be demonstrated in an area efficient footprint.

While the test results collected for this TI Design are focused on a particular PIR sensor part number, it is expected that similar results can be obtained with any similarly specified PIR sensor that is available when the techniques and circuit designs demonstrated in this TI Design are applied.

Lastly, for any PIR sensor, it is necessary to use a lens in front of the sensor to extend the detection range by focusing the infrared energy onto the sensor elements. Using a Fresnel lens, the infrared image for the viewing area is spread across all of the sensor elements. The lens shape and size, therefore, determines the overall detection angle and viewing area. For this TI Design, the Murata IML-0669 lens is used so that a maximum field of view and detection range could be demonstrated. Ultimately, the choice of lens will be determined by the field of view angle and detection range required by the application.

## 2.3 Highlighted Products

The Low-Power PIR Motion Detector Reference Design features the following devices:

- LPV802 ( 2.3.1): Nano-power, CMOS input, rail-to-rail IO operational amplifier
- TLV3691 ( 2.3.2): Nano-power, CMOS input, rail-to-rail input comparator
- CC1310 ( 2.3.3): SimpleLink multi-standard Sub-1 GHz ultra-low-power wireless MCU

For more information on each of these devices, see their respective product folders at [www.TI.com](http://www.TI.com).

### 2.3.1 LPV802

#### Features:

- For  $V_S = 3.3\text{ V}$ , typical unless otherwise noted
  - Supply current at 320 nA
  - Operating voltage range: 1.6 to 5.5 V
  - Low  $TCV_{OS}$  1  $\mu\text{V}/^\circ\text{C}$
  - $V_{OS}$  3.5 mV (max)
  - Input bias current: 100 fA
  - PSRR: 115 dB
  - CMRR: 98 dB
  - Open-loop gain: 120 dB
  - Gain bandwidth product: 8 kHz
  - Slew rate: 2 V/ms
  - Input voltage noise at  $f = 100\text{ Hz}$  340 nV/ $\sqrt{\text{Hz}}$
  - Temperature range:  $-40^\circ\text{C}$  to  $125^\circ\text{C}$

#### Applications:

- Gas detectors (CO and O<sub>2</sub>)
- PIR motion detectors
- Ionization smoke detectors
- Thermostats
- IoT Remote Sensors
- Active RFID readers and Tags
- Portable medical equipment
- Sensor network powered by energy scavenging

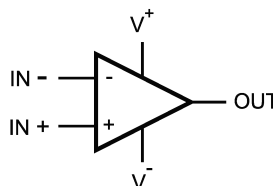


図 2. LPV802 Functional Block Diagram

The LPV802 is a dual nano-power amplifier designed for ultra-long life battery applications. The operating voltage range of 1.6 to 5.5 V coupled with typically 320 nA of supply current per channel make it well suited for remote sensor applications. The LPV802 has a carefully designed CMOS input stage that outperforms competitors with typically 100-fA  $I_{BIAS}$  currents and CMRR of 98 dB. This low input current significantly reduces  $I_{BIAS}$  and  $I_{OS}$  errors introduced in megohm resistance, high impedance photodiode, and charge sense situations. The LPV802 is a member of the PowerWise™ family and has an exceptional power-to-performance ratio.

EMI protection was designed into the device to reduce sensitivity to unwanted RF signals. The LPV802 is offered in the 8-pin VSSOP 3-mm×3-mm package.

### 2.3.2 TLV3691

**Features:**

- Low quiescent current: 75 nA
- Wide supply:
  - 0.9 to 6.5 V
  - $\pm 0.45$  to  $\pm 3.25$  V
- Micro packages: DFN-6 (1 × 1 mm), 5-pin SC70
- Input common-mode range extends 100 mV beyond both rails
- Response time: 24  $\mu$ s
- Low input offset voltage:  $\pm 3$  mV
- Push-pull output
- Industrial temperature range:  $-40^{\circ}\text{C}$  to  $125^{\circ}\text{C}$

**Applications:**

- Overvoltage and undervoltage detection
- Window comparators
- Overcurrent detection
- Zero-crossing detection
- System monitoring:
  - Smart phones
  - Tablets
  - Industrial sensors
  - Portable medical

The TLV3691 offers a wide supply range, low quiescent current 150 nA (maximum), and rail-to-rail inputs. All of these features come in industry-standard and extremely small packages, making this device an excellent choice for low-voltage and low-power applications for portable electronics and industrial systems.

Available as a single channel, its low power, wide supply, and temperature range makes this device flexible enough to handle almost any application from consumer to industrial. The TLV3691 is available in SC70-5 and 1×1-mm DFN-6 packages. This device is specified for operation across the expanded industrial temperature range of  $-40^{\circ}\text{C}$  to  $125^{\circ}\text{C}$ .

### 2.3.3 CC1310

#### Features:

- MCU:
  - Powerful ARM® Cortex®-M3
  - EEMBC CoreMark® score: 142
  - EEMBC ULPBench™ score: 158
  - Up to 48-MHz clock speed
  - 128KB of in-system programmable Flash
  - 8KB of SRAM for cache (or as general-purpose RAM)
  - 20 KB of ultra-low leakage SRAM
  - 2-pin cJTAG and JTAG debugging
  - Supports over-the-air (OTA) upgrade
- Ultra-low-power sensor controller:
  - Can run autonomous from the rest of the system
  - 16-bit architecture
  - 2KB of ultra-low leakage SRAM for code and data
- Efficient code-size architecture, placing TI-RTOS, drivers, *Bluetooth*® low energy controller, IEEE 802.15.4 MAC, and Bootloader in ROM
- RoHS-compliant package:
  - 7x7-mm RGZ VQFN48 (30 GPIOs)
  - 5x5-mm RHB VQFN48 (15 GPIOs)
  - 4x4-mm RSM VQFN48 (10 GPIOs)
- Peripherals:
  - All digital peripheral pins can be routed to any GPIO
  - Four general-purpose timer modules (Eight 16-bit or four 32-bit timers, PWM each)
  - 12-bit ADC, 200 ksps, 8-channel analog MUX
  - Continuous time comparator
  - Ultra-low-power clocked comparator
  - Programmable current source
  - UART
  - 2x SSI (SPI, MICROWIRE, TI)
  - I<sup>2</sup>C
  - I<sup>2</sup>S
  - Real-time clock (RTC)
  - AES-128 security module
  - True random number generator (TRNG)
  - Support for eight capacitive sensing buttons

- Integrated temperature sensor
- External system:
  - On-chip internal DC-DC converter
  - Very few external components
  - Seamless integration with the SimpleLink CC1190 range extender

- Low power:
  - Wide supply voltage range: 1.8 to 3.8 V
  - Active-Mode RX: 5.5 mA
  - Active-Mode TX at 10 dBm: 12.9 mA
  - Active-mode MCU 48 MHz running CoreMark: 2.5 mA (51  $\mu$ A/MHz)
  - Active-mode MCU: 48.5 CoreMark/mA
  - Active-mode sensor controller at 24 MHz:  
0.4 mA + 8.2  $\mu$ A/MHz
  - Sensor controller, one wake up every second performing one 12-bit ADC sampling: 0.85  $\mu$ A
  - Standby: 0.6  $\mu$ A (RTC running and RAM and CPU retention)
  - Shutdown: 185 nA (wakeup on external events)
- RF section:
  - 2.4-GHz RF transceiver compatible with *Bluetooth* Low Energy (BLE) 4.1 specification and IEEE 802.15.4 PHY and MAC
  - Excellent receiver sensitivity –124 dBm using long-range mode, –110 dBm at 50 kbps, –89 dBm at BLE
  - Excellent selectivity: 52 dB
  - Excellent blocking performance: 90 dB
  - Programmable output power up to 14 dBm
  - Single-ended or differential RF interface
  - Suitable for systems targeting compliance with worldwide radio frequency regulations:
    - ETSI EN 300 220, EN 303 131,  
EN 303 204 (Europe)
    - EN 300 440 Class 2 (Europe)
    - FCC CFR47 Part 15 (US)
    - ARIB STD-T108 (Japan)
  - Wireless M-Bus and IEEE 802.15.4g PHY
- Tools and development environment:
  - Full-feature and low-cost development kits
  - Multiple Reference Designs for Different RF Configurations
  - Packet sniffer PC software
  - Sensor Controller Studio
  - SmartRF™ Studio
  - SmartRF Flash Programmer 2
  - IAR Embedded Workbench® for ARM
  - Code Composer Studio™

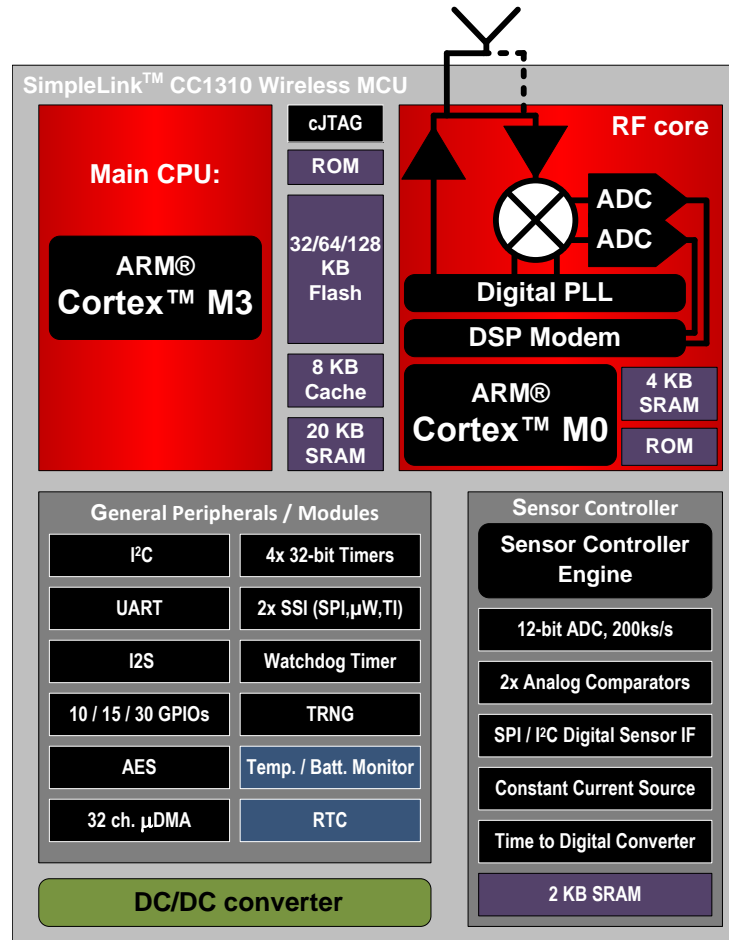


図 3. CC1310 Functional Block Diagram

This device is a member of the CC26xx and CC13xx family of cost-effective, ultra-low-power, 2.4-GHz and Sub-1 GHz RF devices. Very low active RF, MCU current, and low-power mode current consumption provide excellent battery lifetime and allow operation on small coin-cell batteries and in energy-harvesting applications.

The CC1310 is the first part in a Sub-1 GHz family of cost-effective, ultra-low-power wireless MCUs. The CC1310 device combines a flexible, very low-power RF transceiver with a powerful 48-MHz Cortex-M3 MCU in a platform supporting multiple physical layers and RF standards. A dedicated radio controller (Cortex-M0) handles low-level RF protocol commands that are stored in ROM or RAM, thus ensuring ultra-low power and flexibility. The low-power consumption of the CC1310 does not come at the expense of RF performance; the CC1310 has excellent sensitivity and robustness (selectivity and blocking) performance.

The CC1310 is a highly integrated, true single-chip solution incorporating a complete RF system and an on-chip DC-DC converter.

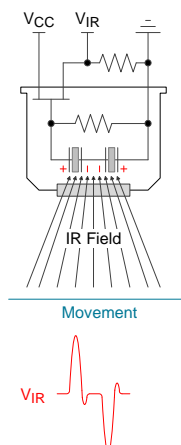
Sensors can be handled in a very low-power manner by a dedicated autonomous ultra-low-power MCU that can be configured to handle analog and digital sensors; thus, the main MCU (Cortex-M3) is able to maximize sleep time.

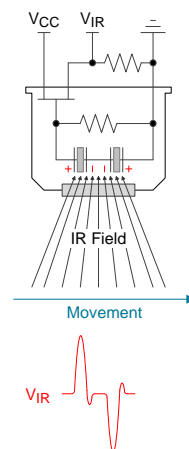
The CC1310 power and clock management and radio systems require specific configuration and handling by software to operate correctly. This has been implemented in the TI SimpleLink CC13x0 SDK, and it is therefore recommended that this software framework is used for all application development on the device. The complete [SimpleLink SDK](#) and device drivers are offered in source code free of charge.

## 2.4 System Design Theory

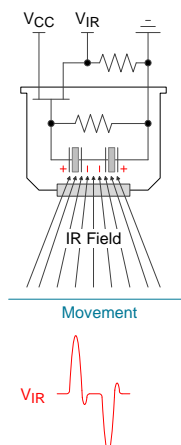
The Low-Power Wireless PIR Motion Detector Reference Design senses motion by detecting differences in infrared (IR) energy in the field of view of the sensor. Because the sensor output is a very small signal, amplification and filtering are necessary to boost the signal and at the same time filter noise so that a representation of the sensor output at a reasonable signal level is obtained while also minimizing false trigger events. The scaled analog output is then converted to digital signals by a window comparator function whose outputs can be used as interrupts to the wireless MCU to save power by only waking up the MCU when it is needed. The following sections discuss the details of the design for these different circuit sections that make up the design's overall subsystem.

### 2.4.1 PIR Sensor

To better understand the circuit, the user must understand how the PIR motion sensor operates. The PIR motion sensor consists of two or more elements that output a voltage proportional to the amount of incident infrared radiation. Each pair of pyroelectric elements are connected in series such that if the voltage generated by each element is equal, as in the case of IR due to ambient room temperature or no motion, then the overall voltage of the sensor elements is 0 V.  shows an illustration of the PIR motion sensor construction.



**図 4. PIR Motion Sensor Illustration**

The lower part of  shows the output voltage signal resulting from movement of a body with a different temperature than the ambient parallel to the surface of the sensor and through the field of view of both sensor elements. The amplitude of this signal is proportional to the speed and distance of the object relative to the sensor and is in a range of low millivolts peak to peak to a few hundred microvolts peak to peak or less. A JFET transistor is used as a voltage buffer and provides a DC offset at the sensor output.

Because of the small physical size of the sensor elements, a Fresnel lens is typically placed in front of the PIR sensor to extend the range as well as expanding the field of view by multiplying and focusing the IR energy onto the small sensor elements. In this manner, the shape and size of the lens determine the overall detection angle and viewing area. The style of lens is typically chosen based on the application and choice of sensor placement in the environment. Based on this information, for best results, the sensor should be placed so that movement is across the sensor instead of straight into the sensor and away from sources of high or variable heat such as AC vents and lamps.

Also note that on initial power up of the sensor, it takes up to 30 s or more for the sensor output to stabilize. During this "warm up" time, the sensor elements are adjusting themselves to the ambient background conditions. This is a key realization in designing this subsystem for maximum battery life in that the sensor itself must be continuously powered for proper operation, which means power cycling techniques applied to either the sensor or the analog signal path itself cannot be applied for proper operation and reliable detection of motion.

## 2.4.2 Analog Signal Path

The analog signal conditioning section is shown in [Figure 5](#). The first two stages in [Figure 5](#) implement the amplified filter function whereas stage 3 implements the window comparator design. Components R10 and C5 serve as a low-pass filter to stabilize the supply voltage at the input to the sensor and are discussed further in [2.4.3](#).

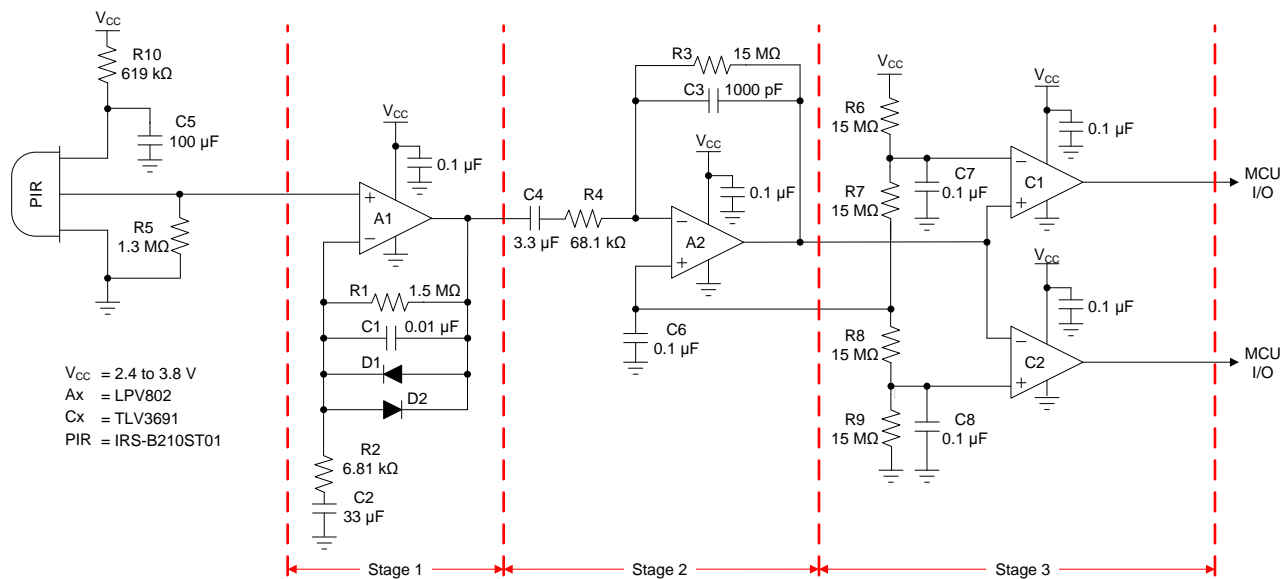


Figure 5. PIR Motion Sensor Analog Signal Path Schematic

Resistor R5 sets the bias current in the JFET output transistor of the PIR motion sensor. To save power, R5 is larger than recommended and essentially current starves the sensor. This comes at the expense of decreased sensitivity and higher output noise at the sensor output, which is a fair tradeoff for increased battery lifetime. Some of the loss in sensitivity at the sensor output can be compensated by a gain increase in the filter stages. Due to the higher gain in the filter stages and higher output noise from the sensor, carefully optimize the placement of the high-frequency filter pole and the window comparator thresholds to avoid false detection.

### 2.4.2.1 Amplified Filter Design

Composed of stages 1 and 2 in [Figure 5](#), the filter section implements a fourth-order band-pass filter using simple poles. Each stage implements identical second-order band-pass filter characteristics. The chosen cutoff frequencies for the band-pass filter are set to 0.7 and 10.6 Hz. The passband gain of each stage is 220 for an overall signal gain of  $\approx 90$  dB and was chosen to maximize the motion sensitivity range for the sensor bias point being used. The data collected for motion sensitivity range at different sensor bias and gain settings is shown in [3.2.2.3.1](#).

Generally, the filter bandwidth must be wide enough to detect a person walking or running by the sensor. At the same time, the filter bandwidth must be narrow to limit the peak-to-peak noise at the output of the filter. In most cases, a bandwidth between 0.3 to 2 Hz is acceptable for this application; however, the use of simple poles means the filter Q is low, which leads to a large filter transition region. With the poles placed this close, the overall passband gain is reduced, which reduces sensitivity and increases the noise floor.

The low-frequency cutoff is critical because it has a major effect on the system noise floor by limiting the overall impact of 1/f noise from the analog front end as well as setting the minimum speed of motion that the system can detect. The practical lower limit on the low-frequency cutoff is due to capacitor sizing at 0.1 Hz. Due to the low bias current being used in the sensor for this TI Design, the low-frequency noise will be worse than a normal higher current design, which means the low-frequency cutoff must be higher than 0.3 Hz. Given a practical range of the low-frequency cutoff to be between 0.3 to 1 Hz, this design uses a low-frequency cutoff in the middle of this range.

The high-frequency cutoff is mostly for reducing broadband noise. The range for its placement is a decade higher than the low-frequency cutoff up to the bandwidth limit set by the open-loop bandwidth of the op amp being used. In this case, the LPV802 has a unity gain bandwidth (UGBW) of 8 kHz, which means for a maximum stage gain of 220, the bandwidth is limited to 36 Hz. Allowing for component tolerances and variation in the UGBW of the LPV802, a practical range for the high-frequency cutoff is between 7 and 14 Hz. Again, the choice was made to use a high-frequency cutoff in the middle of this range.

The first stage of the filter is arranged as a non-inverting gain stage. This provides a high-impedance load to the sensor so its bias point remains fixed. Because this stage has an effective DC gain of one due to C2, the sensor output bias voltage provides the DC bias for the first filter stage. Feedback diodes, D1 and D2 provide clamping so that the op amps in both filter stages stay out of saturation for motion events, which are close to the sensor. 式 1 to 式 3 show the gain and cutoff frequencies for this stage:

$$f_{\text{Low1}} = \frac{1}{2\pi \times R2 \times C2} = \frac{1}{2\pi \times 6.81 \text{ k}\Omega \times 33 \text{ }\mu\text{F}} = 0.71 \text{ Hz} \quad (1)$$

$$f_{\text{High1}} = \frac{1}{2\pi \times R1 \times C1} = \frac{1}{2\pi \times 1.5 \text{ M}\Omega \times 0.01 \text{ }\mu\text{F}} = 10.6 \text{ Hz} \quad (2)$$

$$|G_1| = 1 + \frac{R1}{R2} = 1 + \frac{1.5 \text{ M}\Omega}{6.81 \text{ k}\Omega} = 221.26 \quad (3)$$

Because the second stage is AC coupled to the first stage, it is arranged as an inverting gain stage. This allows the DC bias to be set to  $V_{CC}/2$  easily by connecting the center point of the divider string in the window comparator to the non-inverting input of the op amp in this filter stage. Because the peak-to-peak noise is present at the output of this stage, R3 is made as large as possible to minimize the dynamic current of the system. 式 4 to 式 6 show the gain and cutoff frequencies for this stage:

$$f_{\text{Low2}} = \frac{1}{2\pi \times R4 \times C4} = \frac{1}{2\pi \times 68.1 \text{ k}\Omega \times 3.3 \text{ }\mu\text{F}} = 0.71 \text{ Hz} \quad (4)$$

$$f_{\text{High2}} = \frac{1}{2\pi \times R3 \times C3} = \frac{1}{2\pi \times 15 \text{ M}\Omega \times 1000 \text{ pF}} = 10.6 \text{ Hz} \quad (5)$$

$$|G_2| = \left| -\frac{R3}{R4} \right| = \left| -\frac{15 \text{ M}\Omega}{68.1 \text{ k}\Omega} \right| = 220.26 \quad (6)$$

The total circuit gain (not including any gain reduction due to pole placement) is given by  $G1 \times G2 = 221.26 \times 220.26 = 48810 = 93.77 \text{ dB}$ . 図 6 and 図 7 show simulation results for these two filter stages.

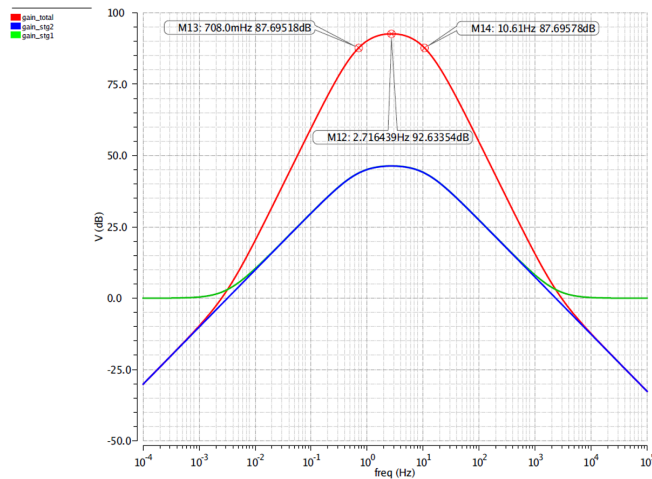


図 6. Amplified Filter Simulation Results (Ideal)

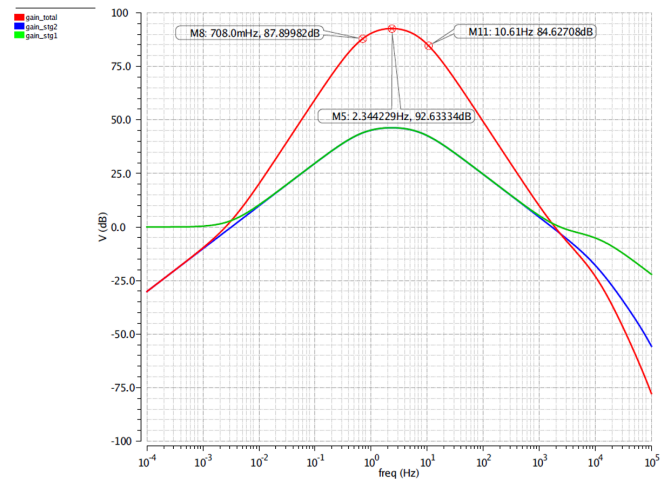


図 7. Amplified Filter Simulation Results (Nonideal)

The responses shown in 図 6 and 図 7 illustrate the effect of finite UGBW for the amplifiers in the circuit. Note that not only is the high-frequency response altered, but also the attenuation at the high-frequency cutoff is increased and the peak gain frequency is shifted slightly.

### 2.4.2.2 Window Comparator Design

The window comparator circuit shown in stage 3 of 図 5 converts the analog output of the filter to digital signals, which are used as interrupts to the MCU to tell it when motion has been detected. Composed of resistors R6 through R9, the resistor divider sets up the thresholds that determine a valid motion detection from the sensor. To save power, this resistor divider also provides the bias voltage for the second stage of the filter. Capacitors C6, C7, and C8 are necessary to stabilize the threshold voltages to prevent chatter at the output of the comparators. These capacitors do not need to be a large value due to the large resistors being used in the resistor divider, but they must be low ESR and low leakage, with ceramic being preferred.

The comparator chosen for this reference design is the TLV3691 due to its ultra-low supply current requirements. The TLV3691 comparator also has rail-to-rail input capability with an input common-mode range that exceeds the supply rails by 100 mV. This is not required for this TI Design, but it does allow the ability to maximize the adjustment range of the window comparator thresholds. The comparator outputs are low when there is no motion detected. Typically, motion across the sensor generates a high pulse on one comparator output followed by a high pulse on the other comparator, which corresponds to the amplification of the S-curve waveform shown in the lower part of 図 4. Which comparator triggers first depends on the direction of the motion being detected.

式 7 and 式 8 are used to adjust the window comparator thresholds:

$$V_{REF\_High} = V_{CC} \frac{R7 + R8 + R9}{R6 + R7 + R8 + R9} = 0.75 \times V_{CC} \tag{7}$$

$$V_{REF\_Low} = V_{CC} \frac{R9}{R6 + R7 + R8 + R9} = 0.25 \times V_{CC} \tag{8}$$

There is also a constraint that  $R6 + R7 = R8 + R9$  so that the  $V_{CC}/2$  bias level is maintained at the center tap of the divider for use as the bias for the second stage of the filter.

The thresholds chosen for this design are a balance between sensitivity and noise immunity. Widening of the window improves noise immunity but reduces sensitivity. Making the window too small can lead to false triggers due to the peak-to-peak noise seen at the input to the window comparator.

### 2.4.3 Power Supply Design

Because of the increasing battery impedance over the life of the battery supply and the low-power supply rejection of the PIR sensor, it is important to design the power supply network to prevent current spikes generated by the MCU from causing false triggers through the analog signal path. While the algorithm implemented in firmware helps to filter such problems, this unwanted power supply feedback loop can become an issue. Ideally, the sensor supply is regulated to break this loop; however, in this design, the extra quiescent current of a regulator reduces battery life, so other methods are explored.

Figure 8 shows a simplified schematic of the power supply network. The PMOS transistor is used in place of the traditional Schottky diode for reversed battery protection. Because the peak currents are in the 30-mA range when the radio transmits, using a low  $R_{DS,ON}$  PMOS provides a much lower voltage drop compared to a Schottky diode, which helps to maximize battery life by allowing the battery to decay to a lower voltage before the circuit is no longer able to function (for more on this technique, see the application report [Reverse Current/Battery Protection Circuits](#)).

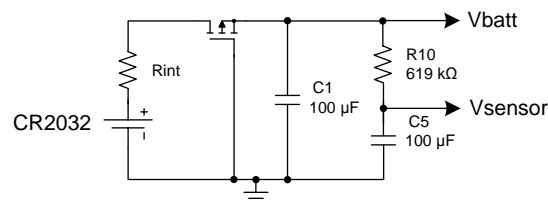


Figure 8. PIR Motion Sensor Simplified Power Supply Network Schematic

Capacitor  $C1$  supplies the circuit during periods of high and fast peak current demand, which helps to maximize the battery capacity and minimize voltage droop on the power supply rail, especially as the battery approaches its end of life and its internal impedance increases (represented by  $R_{int}$  in Figure 8). The calculation for  $C1$  is provided in Equation 9. For more details on this calculation and the effects of high-current peaks on battery life and capacity, see the white paper [Coin cells and peak current draw](#).

$$C1 = \frac{\Delta Q}{V_{MAX} - V_{MIN}} \quad (9)$$

where:

- $\Delta Q = Q_{dis} - \frac{V_{MIN}}{R_{int}} t_{tot}$
- $Q_{dis} = \sum j_n \times t_n$

$V_{MAX}$  is the voltage across the capacitor at the start of the current pulse at the end of the battery's life, and  $V_{MIN}$  is the circuit operating minimum, which is the sensor minimum plus the voltage drop across  $R10$  due to the sensor bias current ( $2 \text{ V} + 0.6 \mu\text{A} \times 619 \text{ k}\Omega \approx 2.4 \text{ V}$ ).  $V_{MAX}$  is taken to be 2.698 V assuming an unloaded end of life battery voltage of 2.7 V ( $V_P$ ). Based on the measured current profile during a radio transmission, shown in Equation 10 and Equation 11:

$$Q_{dis} = 23.2 \text{ mA} \times 100 \mu\text{s} + 4 \text{ mA} \times 3.5 \text{ ms} + 8.8 \text{ mA} \times 2.5 \text{ ms} = 38.32 \mu\text{C} \quad (10)$$

For  $C1$ :

$$C1 = \frac{38.32 \mu\text{C} - \frac{2.4 \text{ V}}{1 \text{ k}\Omega} \times 6.1 \text{ ms}}{2.698 \text{ V} - 2.4 \text{ V}} = 79.5 \mu\text{F} \quad (11)$$

This design uses  $C1 = 100 \mu\text{F}$  and additional decades of capacitors in parallel for improved impedance at higher frequencies. The time required to recharge the composite  $C1$  capacitor after the high-current event is given in 式 12 and is sufficiently low compared to the active and standby states of the device where current consumption is in the low-microamp range.

$$t = R_{\text{int}} \times C1 \times \ln\left(\frac{V_p - V_{\text{MIN}}}{V_p - V_{\text{MAX}}}\right) = 1 \text{ k}\Omega \times 111.514 \mu\text{F} \times \ln\left(\frac{2.7 \text{ V} - 2.4 \text{ V}}{2.7 \text{ V} - 2.698 \text{ V}}\right) = 0.56 \text{ s} \quad (12)$$

With the value of  $C1$  determined,  $R10$  and  $C5$  can be sized to prevent false triggers from occurring during high-current events on the power supply. With  $R10$  chosen based on the acceptable amount of voltage drop due to the sensor bias,  $C5$  was determined experimentally. If desired,  $R10$  can be reduced in value to be able to operate at slightly lower voltage; however, the time constant for  $R10$  and  $C5$  shown in 図 8 needs to be maintained. This means  $C5$  becomes larger and requires a different dielectric, which in all likelihood would be more leaky or more costly and negate some of the advantage to reducing  $R10$ . Similar to what was done for  $C1$ ,  $C5$  has additional decades of capacitors in parallel to maintain a low impedance at higher frequencies.

2.4.4 Firmware Control

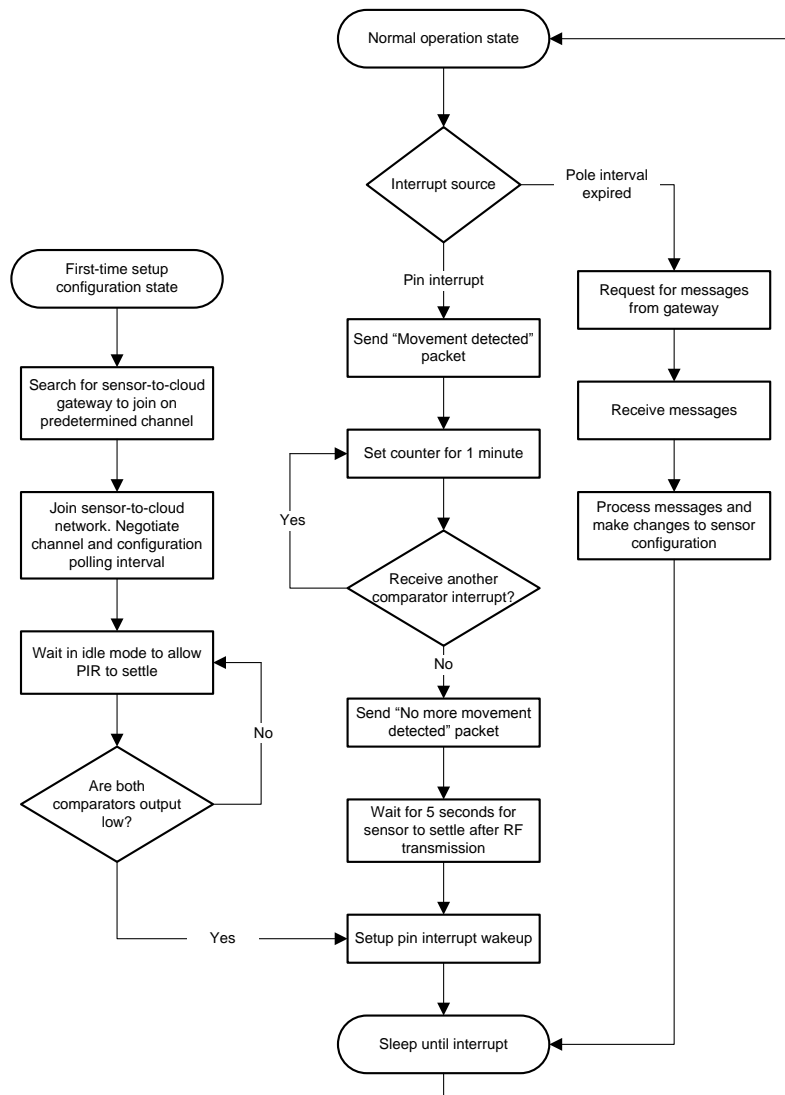


図 9. Wireless PIR Firmware Flow Chart

The flow chart shown in 図 9 describes the CC1310 operation in this TI Design. The CC1310 first starts by checking the source of the wake-up. If the device is woken up by reset, the system is powered on for the first time. The CC1310 searches for the sensor-to-cloud gateway to join, then after joining waits in idle mode to allow the PIR sensor and analog signal chain to power on and allow the operating point to settle. After the comparator output has settled low, any where from 30 seconds to 2 minutes depending on the device, the firmware looks at the outputs of the window comparator. By default, the output of both comparators must be low. Once the PIR sensor and analog signal chain are functioning correctly, the CC1310 enters sleep mode.

The CC1310 stays in sleep mode until the PIR sensor signals the MCU that motion is detected by means of the window comparator outputs serving as interrupts. When the CC1310 is woken up by the PIR sensor, it sends a "motion detected" packet to notify the host controller that motion has been detected. The CC1310 waits until the PIR sensor is silent for one minute before sending an "all clear" packet to the host controller and returning to shutdown mode. Also as per the TI 15.4 stack, the CC1310 wakes up on the configuration polling interval set by the gateway to check if there are any messages from the gateway. During this time, the sensor and gateway can negotiate a new frequency when frequency hopping is enabled.

#### 2.4.5 Polling Intervals and Frequency Hopping

To increase battery life the Low-Power Wireless PIR Motion Detector Reference Design does not currently implement a frequency hopping scheme. A frequency hopping device will lose synchronization if it does not get any collector data/ack within about 20 minute for the default 250 ms dwell interval. In frequency hopping mode, an end device shall track the slot boundaries of collector and the synchronization is maintained based on timing information on received Data/ACK. For the default 250 ms dwell time parameter, it is imperative that a data /ack from collector is received at least once within 20 minutes. It is recommended to either transmit a poll (and received ACK/Data from collector) or data (and receive ACK) within this period.

### 3 Hardware, Firmware, Testing Requirements, and Test Results

#### 3.1 Required Hardware and Firmware

##### 3.1.1 Hardware

Figure 10 shows the hardware for the Low Power Wireless PIR Motion Detector Reference Design Enabling Sensor-to-Cloud Networks. The printed circuit board (PCB) is in a 35x75-mm rectangular form factor and comes with 0.5-in nylon standoffs to ensure ease of use while performing lab measurements.

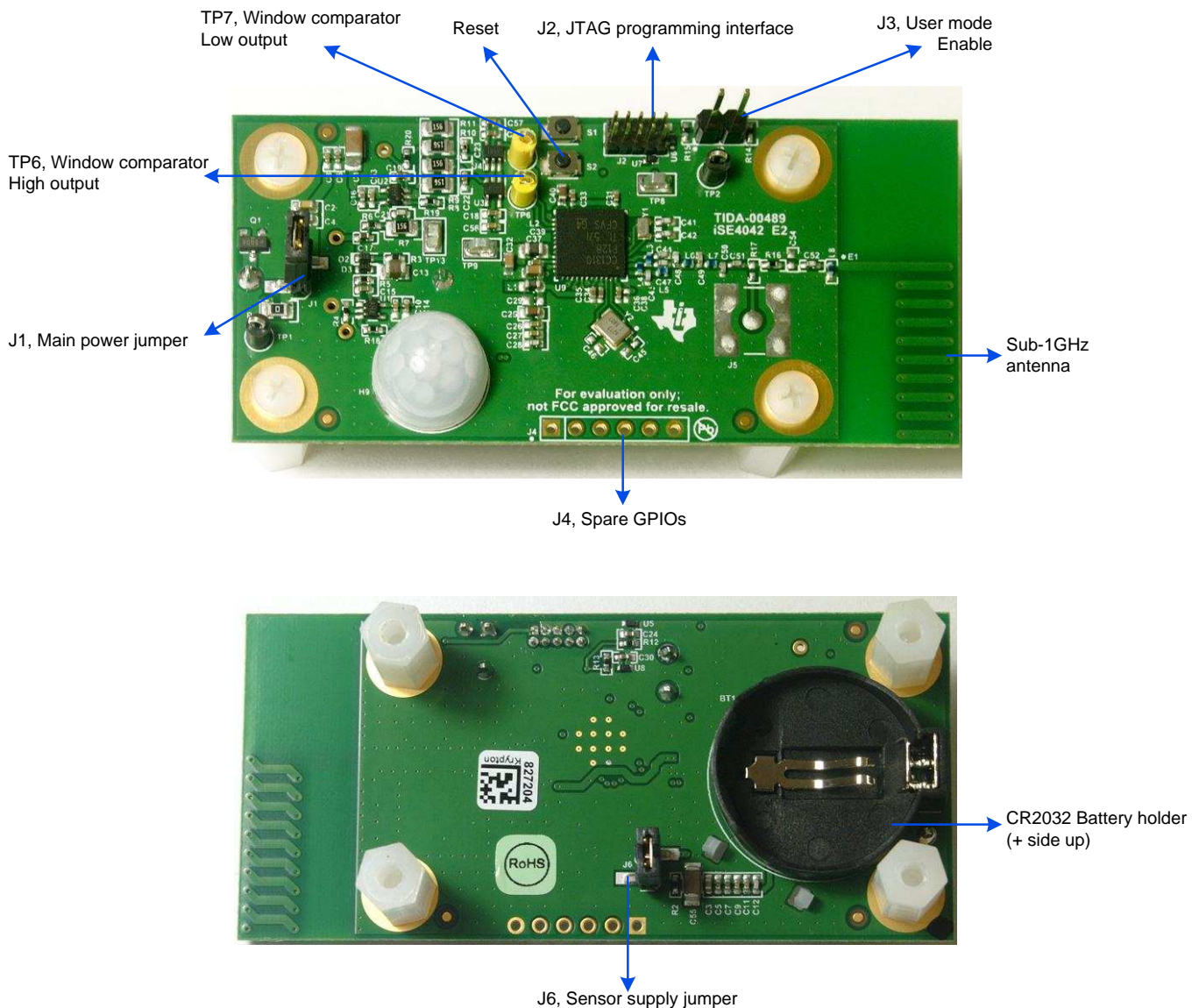


Figure 10. Hardware Description of Low-Power Wireless PIR Motion Detector Reference Design

All the integrated circuits (CC1310, LPV802, and TLV3691), several test points, and jumpers are located on the top side of the PCB. The antenna is also located on the top side of the PCB.

The bottom side of the PCB contains the CR2032 coin cell battery holder, jumper J6, and the bottom half of the antenna.

There are four unused GPIOs that have been brought out from the CC1310 to an unpopulated header to facilitate future prototyping and debugging.

### 3.1.1.1 Jumper Configuration

To facilitate measuring critical parameters and debugging in this reference design, there are several jumpers included. However, to properly operate the design, these jumpers must be installed correctly. The jumper configuration for normal operation is as follows: J1 = Shorted, J2 = Open, J3 = Open, J6 = Shorted. The jumper configuration to program the CC1310 is as follows: J1 = Open (power applied to Pin 2), J2 = Connected through ribbon cable to the SmartRF06 Evaluation Board (EVM), J3 = Open, J6 = Don't care.

See [Figure 10](#) for a brief description of the intended function of these different jumpers.

### 3.1.1.2 Test Point Description

This design includes several test points to monitor critical signals. The following is a brief description of these test points:

- TP1, TP2: Ground points for probes or common points for voltage measurements
- TP6, TP7: Window comparator high threshold and low threshold outputs, respectively
- TP8: Filtered battery supply forming input to the DC-DC converter in the CC1310
- TP9: Filtered DC-DC converter output from the CC1310
- TP13: Output of analog filter stage, which is also the input to the window comparator stage

### 3.1.1.3 Gateway Hardware

The first option for demonstrating the sensor-to-cloud system is to build TI's [Sub-1 GHz Sensor to Cloud Industrial IoT Gateway Reference Design](#). The following items are required to build the sensor-to-cloud gateway:

- A [CC1310](#) or [CC1350](#) LaunchPad™ to run the MAC coprocessor application
- An AM335x-based [BeagleBone Black](#) board
- A 5-V power supply for the BeagleBone Black
- [BeagleBone Black wireless connectivity cape](#) to connect the gateway to the Internet
- An 8GB microSD card (the TI processor SDK image requires at least 8GB of space)
- A means to configure and set up the BeagleBone Black microSD card (Windows® or Linux machine)
- A PC to host and run the web browser used to view the web application
- A USB cable to connect the BeagleBone Black with the CC1310 or CC1350 LaunchPad

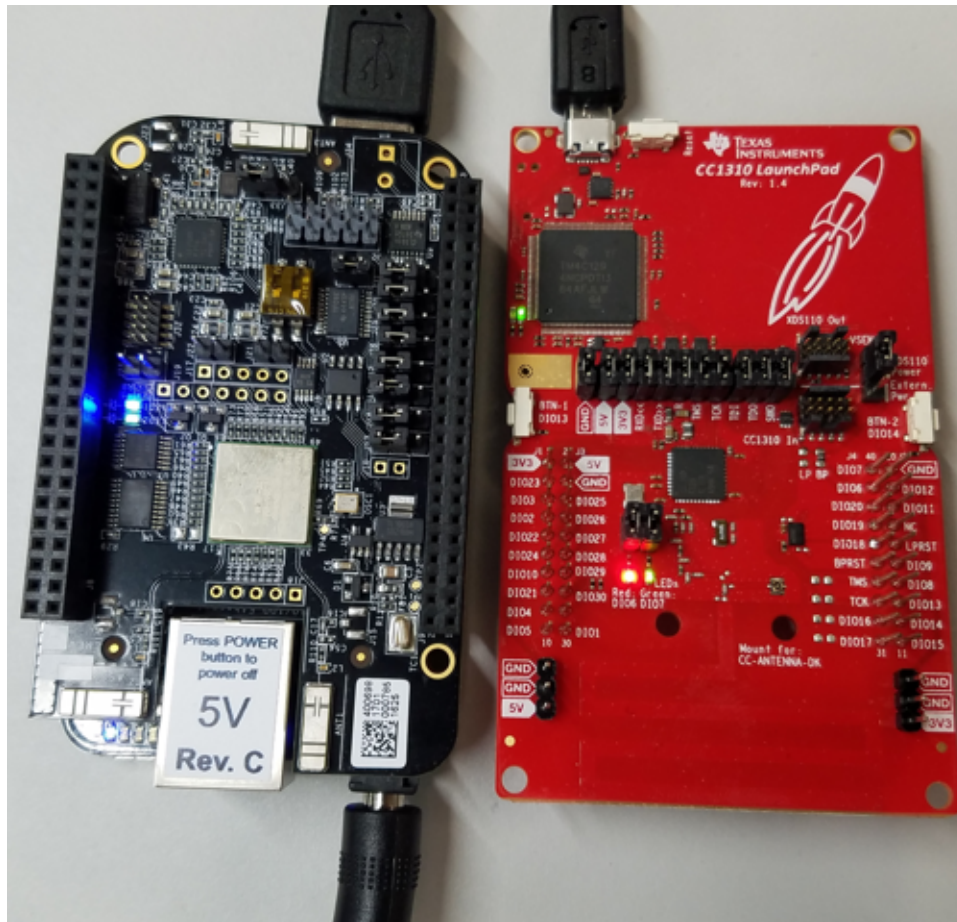


図 11. BeagleBone Gateway Hardware Setup

### 3.1.1.4 Collector Hardware

The second and easier option for demonstrating the sensor-to-cloud system is to use a CC1310 or CC1350 LaunchPad running the Collector Example Application featured in the [SimpleLink SDK](#) to act as the gateway device. The LaunchPad creates the TI 15.4-Stack network, allows sensor devices to join the network, collects sensor information sent by devices running the sensor example application, and tracks if the devices are on the network or not by periodically sending tracking request messages. The only hardware required is the LaunchPad and a PC to view the UART output.

### 3.1.1.5 Miscellaneous

Note that due to the number of sensitive high impedance nodes in this design, probing points aside from the ones with dedicated test points should be done so with the probe impedance in mind.

An example of this would be the probing of the reference inputs to the window comparator. Because these reference thresholds are generated from a resistor divider composed of four 15-M $\Omega$  resistors, using a standard oscilloscope probe or voltmeter with a 10-M $\Omega$  input impedance effectively loads the circuit being measured and provides a false measurement.

### 3.1.2 Firmware

#### 3.1.2.1 Loading Firmware

The firmware used on this TI Design was developed using TI's [Code Composer Studio \(CCS\)](#) software (version 7.1.0). The IAR Embedded Workbench for ARM also supports the CC13xx line of SimpleLink products.

Powering the board from 3.0 V is also necessary and is supplied at pin 2 of Jumper J1. Connecting the external power source at this location bypasses the reversed battery protection.

The TI Design hardware is programmed by connecting the 10-pin mini ribbon cable from J2 to the SmartRF06 EVM (10-pin ARM Cortex Debug Connector, P410). See [Figure 12](#) for a photo of the correct setup for connecting the TI Designs hardware to the SmartRF06 EVM.

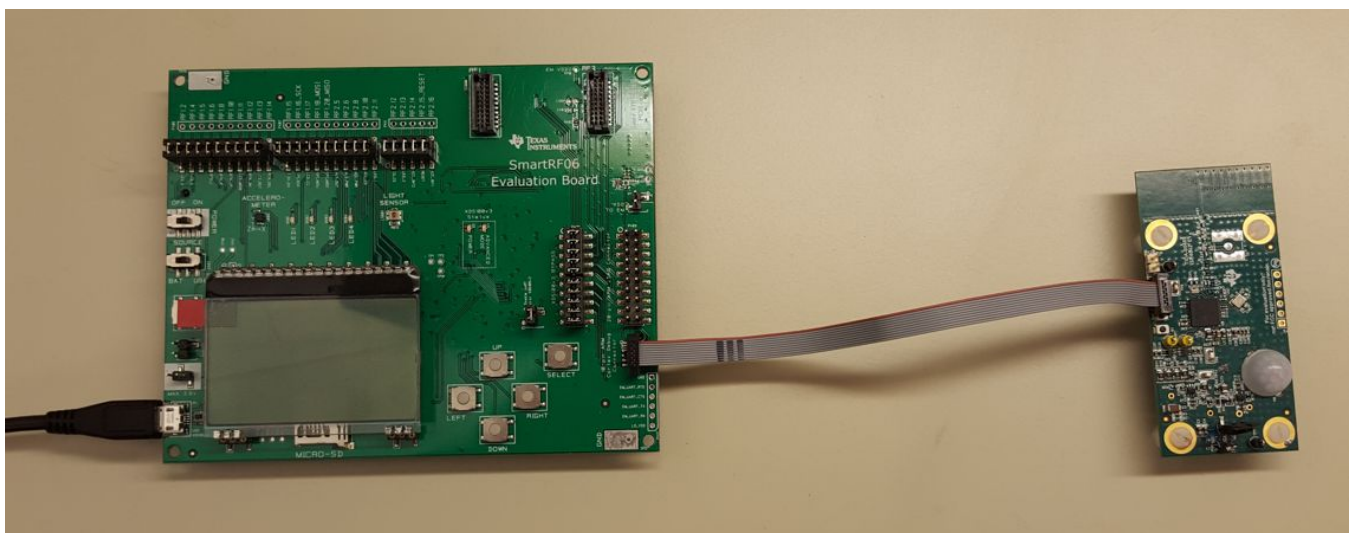


**Figure 12. Connection of SmartRF06 Evaluation Board and TI Designs Hardware for Programming and Debugging**

To run the LaunchPad collector, connect the CC13xx LaunchPad to the PC and open a serial connection to the application UART. To restart the collector, hold BTN-2 while pressing the reset button. Press the BTN-2 button on the LaunchPad collector to allow new devices to join the network. Press the BTN-2 a second time to close the network, which does not allow new devices to join the network.

```

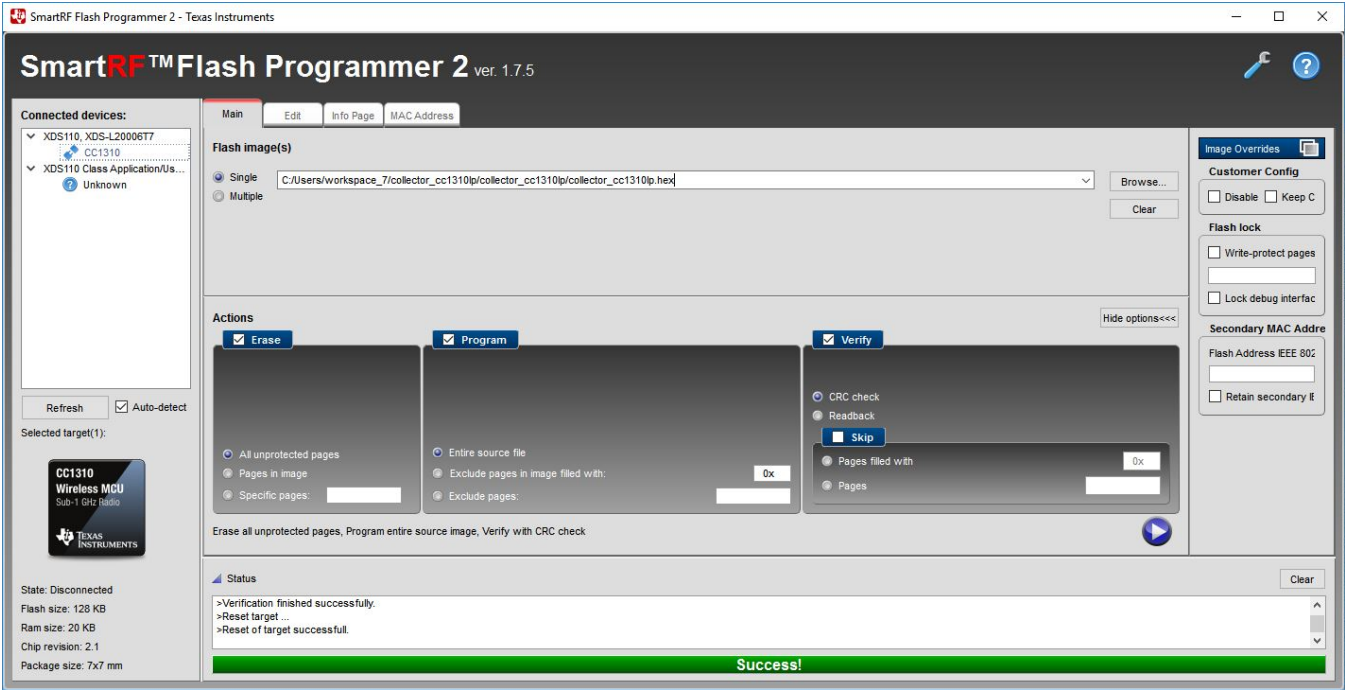
COM8:115200baud - Tera Term VT
File Edit Setup Control Window Help
TI Collector
Restarted
Channel: 32
PermitJoin-ON
Joined: 0x1
Sensor 0x1
ConfigRsp: 0x1
PermitJoin-OFF

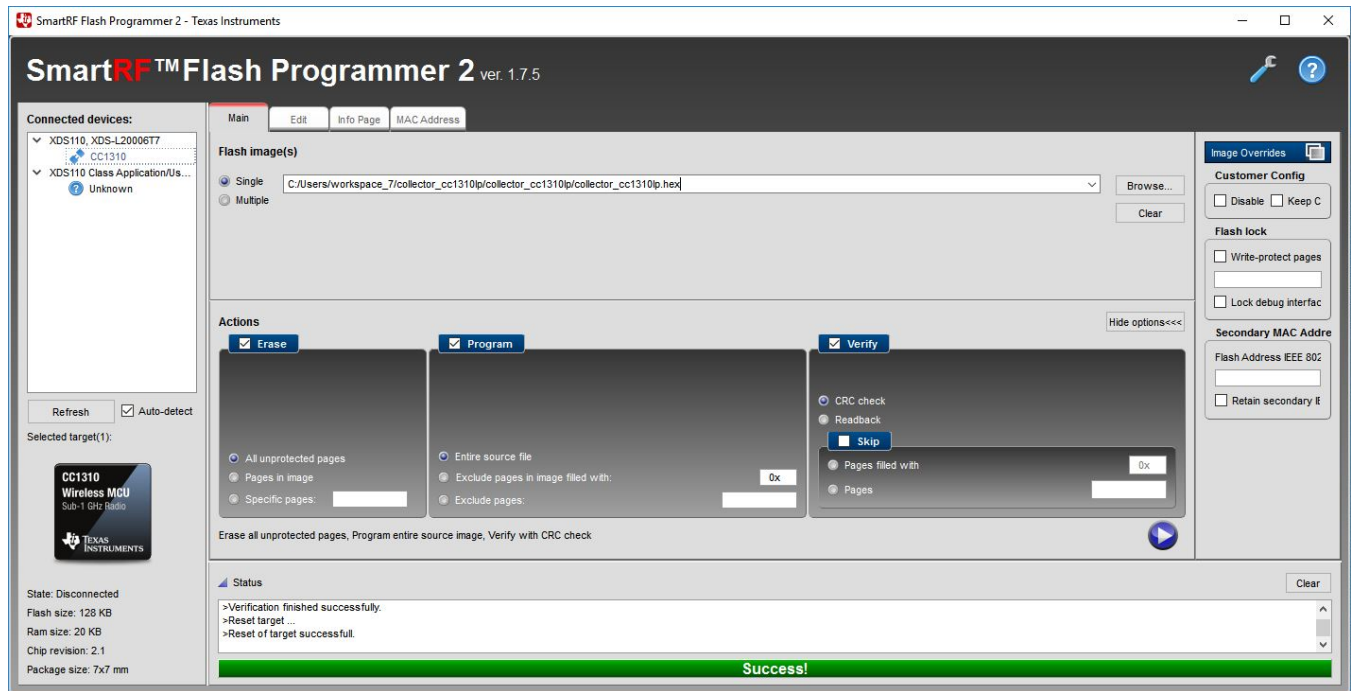
```

**Figure 13. CC1310 LaunchPad Collector UART Output**

### 3.1.2.2 Programming the Collector

The SimpleLink SDK download includes a quick start guide to program and run the TI 15.4 Stack collector. The guide are in the SimpleLink SDK installation directory under docs (for example, "C:\ti\simplelink\_cc13x0\_sdk\_1\_30\_00\_06\docs\ti154stack"). Open the Software Developers Guide and navigate to Example Applications on the left side bar.

Flash Programmer 2 is the easiest way to program the collector if .hex files are already generated. CCS can be used to make changes to the example code.  14 shows the Flash Programmer settings after plugging in the LaunchPad.



 14. Flash Programmer 2 Setup

### 3.1.2.3 Receiving Data Packets

As this reference guide previously describes, this TI Design is programmed to detect a person's presence by using the PIR sensor (see 2.2.5 and 2.4.1). The CC1310 broadcasts three possible action values:

- A "Request for Data" packet when the polling interval timer has expired
- A "Motion Detected" packet when the first motion is detected (see [Figure 15](#))

2208.995608	0x0001	0xaabb	TI 802.15.4GE	51Data, Dst: 0xaabb, Src: 0x0001
2209.007615			TI 802.15.4GE	7Ack

›Frame Check Sequence (TI CC24xx format): 0x80e4: FCS OK

•Data (20 bytes)

Data: 057443fb08004b120050000120bf0200804f1200

**Figure 15. Motion Detected Packet Data**

- An "All Clear" packet one minute after the last motion is detected (see [Figure 16](#))

2269.277551	0x0001	0xaabb	TI 802.15.4GE	51Data, Dst: 0xaabb, Src: 0x0001
2269.289693			TI 802.15.4GE	7Ack

›Frame Check Sequence (TI CC24xx format): 0x80e4: FCS OK

•Data (20 bytes)

Data: 057443fb08004b120050000120bf0200804f1200

[Length: 20]

**Figure 16. All Clear Packet Data**

To verify the proper operation of the radio transmission, a CC1350 or CC1310 LaunchPad board can be used as a packet sniffer device for TI 15.4-Stack radio packets. This feature enables easier development and debugging for those developing products with the TI 15.4-Stack. The TI 15.4-Stack installs the TiWSPc2, which uses TI hardware to capture OTA data before sending the packets to Wireshark or a PCAP file, and provides .dll files to dissect packets that follow the TI 802.15.4ge protocol to Wireshark. [Figure 17](#) is an example of TI 15.4-Stack-based application OTA traffic being presented as a Wireshark capture.

### 3.1.2.3.1 CC13xx LaunchPad Sniffer

The SimpleLink SDK download includes quick start guides to install, program and run the TI 15.4 Stack sniffer (for example, "C:\ti\simplelink\_cc13x0\_sdk\_1\_30\_00\_06\docs\ti154stack"). Open the Software Developers Guide and navigate to Example Applications on the left side bar. All the required software except for Wireshark is downloaded within the SimpleLink SDK.

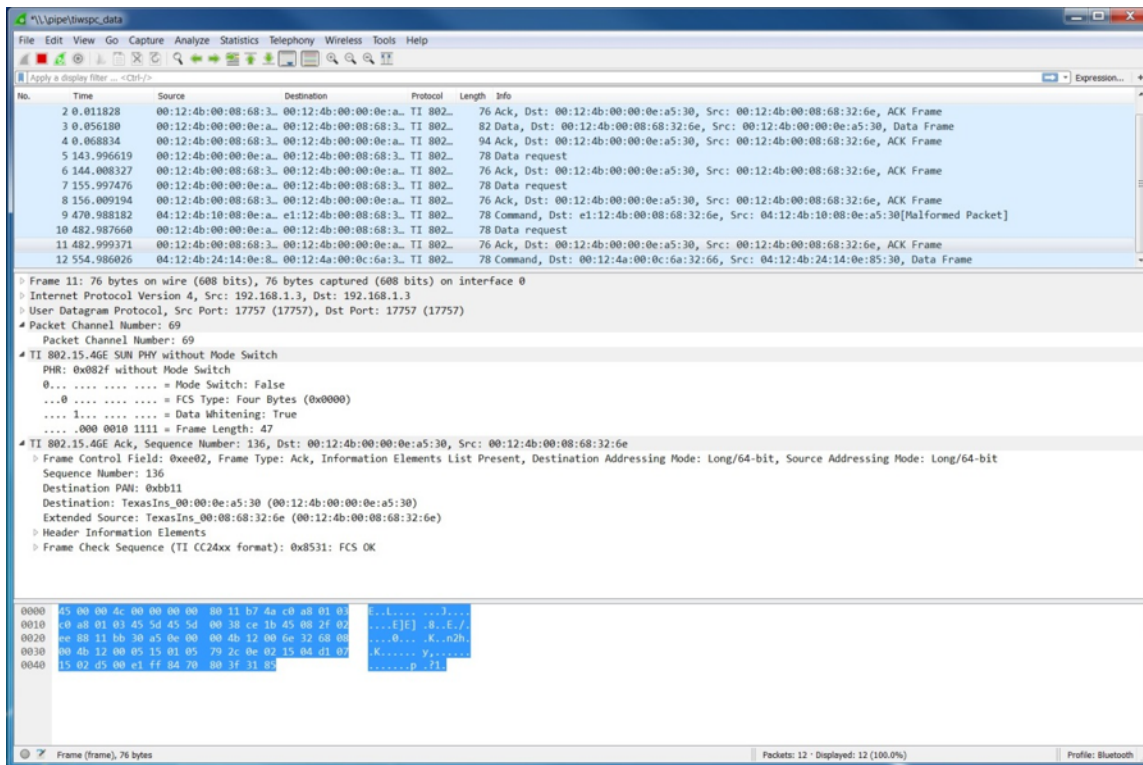


図 17. Wireshark Packet Sniffer Software

Choose a packet to get detailed information on the data in that packet. The installed .dll file lets Wireshark dissect the information in a TI 802.15.4GE packet for easy debugging.

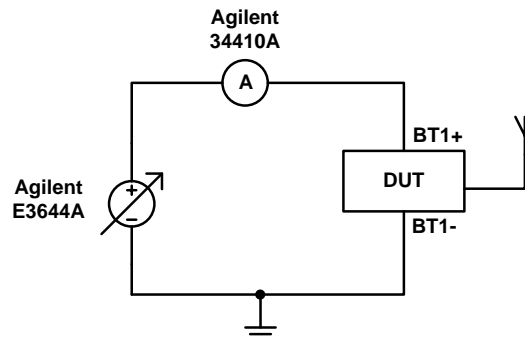
## 3.2 Testing and Results

### 3.2.1 Test Setup

The Low-Power Wireless PIR Motion Detector Reference Design Enabling Sensor-to-Cloud Networks is characterized to support all of the critical specifications for this subsystem. The following subsections describe the test setups for these measurements, including the equipment used and the test conditions unless otherwise noted.

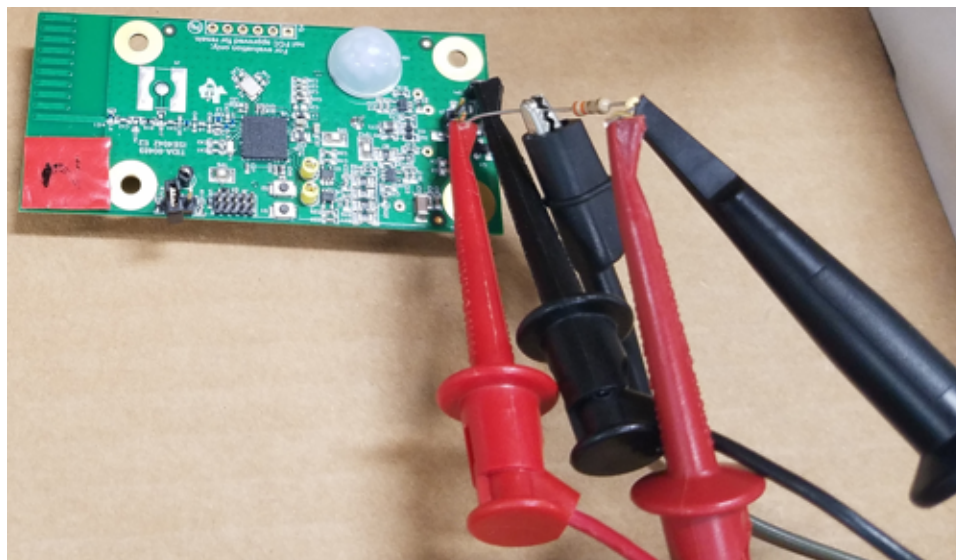
### 3.2.1.1 Power Consumption

The power consumption measurements for this reference design are critical in balancing battery lifetime with sensor bias current and motion sensitivity. An initial prototype allowed measurements of the different current paths in the design as a preliminary analysis. The results from that prototype are shown in 3.2.2.1. Measurements of supply current were then performed on the reference design hardware, which confirmed the prototype measurements. Further characterization was done on the reference design hardware over the voltage range of the design. The test setup for the supply current measurements is illustrated in 18.



18. Test Circuit Used for Measuring Supply Current

To compute the battery life, the radio transmission intervals also need to be characterized as these intervals have brief periods of high peak currents before settling to the low microamp current levels measured using the setup in 18. The measurement of the radio transmission interval involves using a sense resistor that interfaces to an oscilloscope, which can then be used to trigger on the high current events. Data from this interval is then exported to Microsoft® Excel® to analyze the data. This setup is illustrated in 19. A 3.4-Ω sense resistor was placed in series with the power supply on the positive battery terminal. Oscilloscope probes were then attached to each side of the resistor to capture the current waveform during transmission.



19. Sense Resistor Used to Measure Supply Current During Radio Transmission Intervals

### 3.2.1.2 **Functional**

The following subsections describe the tests for functionality under various environmental conditions. These tests generally verify the limits of operation for the subsystem.

#### 3.2.1.2.1 **Temperature and Humidity Range**

This TI Design was stressed under temperature and humidity bias to ensure the design operates and does not produce false triggers under extremes of the targeted environment. The typical extended building environment temperature range is assumed to be 0°C to 50°C while additional testing was performed to test the limits of the design down to –30°C and up to 60°C. Similarly, the typical humidity range for a building environment is assumed to be 20% to 70%.

The chamber used for the temperature and humidity stress was the CSZ ZH322-H/AC Temperature and Humidity Chamber and a Vaisala® HMP235 Humidity Probe to monitor humidity. A Watlow® F-4 Controller was used to automate the testing. The reference design PCB was placed in the chamber with a new Energizer® CR2032 lithium-ion coin cell battery installed. The CC1111 USB dongle was placed near the TI Design hardware inside the chamber and connected to a laptop outside of the chamber with a USB cable to monitor for false triggers during the test. [Figure 20](#) shows a picture of the setup.



**Figure 20. Wireless PIR Motion Detector Temperature and Humidity Test Setup**

To prevent false detection due to rapid changes in ambient temperature and subsequent sensor settling, the temperature was slowly ramped during the test as would be expected in a typical operating environment. The test was started with a 10-minute soak at 25°C followed by a 1°C per minute ramp up to 50°C with a 5-minute soak, followed by a 5°C per minute ramp to 60°C, and back down to 50°C with a 5-minute soak at 50°C, followed by a 1°C per minute ramp down to 0°C with a 5-minute soak. At 0°C, a similar 5°C per minute ramp was applied down to –30°C and back up to 0°C with a 5-minute soak at 0°C, followed by a 1°C per minute ramp back up to 25°C.

Because of the physical construction of the chamber and its use of fans for air flow within the chamber, false triggers were observed during the temperature ramping periods. During the soaking periods, false triggering subsided over the entire temperature range tested, which proves the functionality of the design over the temperature extremes. This observation is common for PIR-based motion detectors and for this reason are generally not recommended for installation near ventilation. The only known way to prevent the false triggering during this test is to cover the sensor so it could not be affected by thermal gradients due to forced air flow and reflections off the walls of the chamber; however, this was not done as part of this measurement.

To prevent false detection due to rapid changes in humidity, the humidity was slowly ramped during the test as would be expected in a typical operating environment. The test consisted of applying a 1% per minute ramp from 20% to 70% and then back down to 20% with a 30-minute initial soak. The temperature was held at 45°C to prevent condensation; however, condensation was observed at 68% and higher humidity points.

The only anomaly observed during this test was at the point where condensation formed on the PCB, which produced false triggering. As the humidity dropped to a point where the PCB dried, the false triggering stopped and was not observed for the remainder of the test.

### **3.2.1.2.2 Motion Sensitivity**

The motion sensitivity range was measured by connecting a dual pulse stretcher design built on a generic prototyping PCB with LED outputs on each channel for visual indication. The inputs to the pulse stretcher are connected to the window comparator output test points of the reference design. Using this method, the PIR sensor was allowed to remain stationary at a fixed location while the LEDs indicate when motion is being detected. The pulse stretcher was powered using its own coin cell battery so that it does not interfere with or modify the operation of the PIR sensor being tested. The farthest distance at which reliable detection of motion was indicated was then measured and reported as the motion sensitivity. Pictures of this setup are shown in [Figure 21](#).

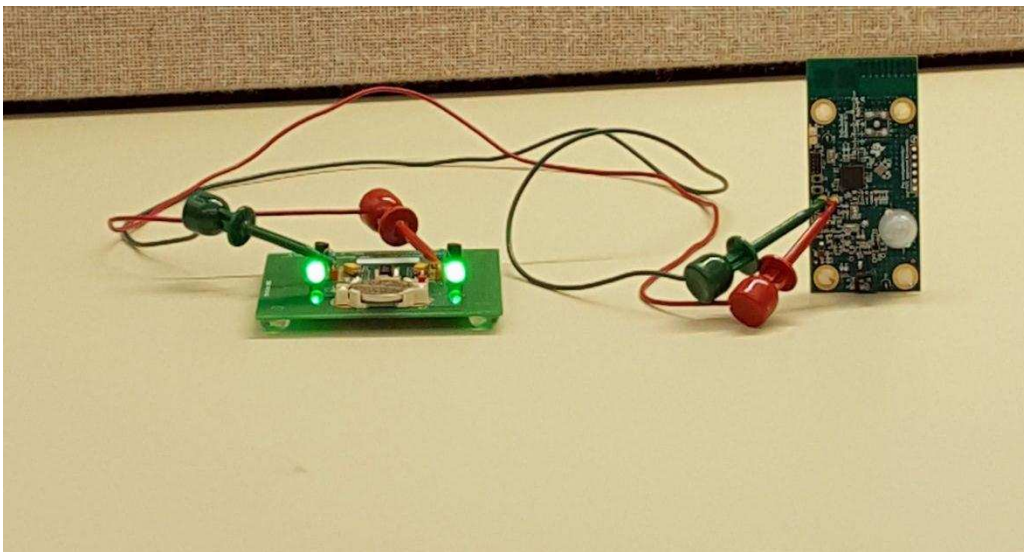
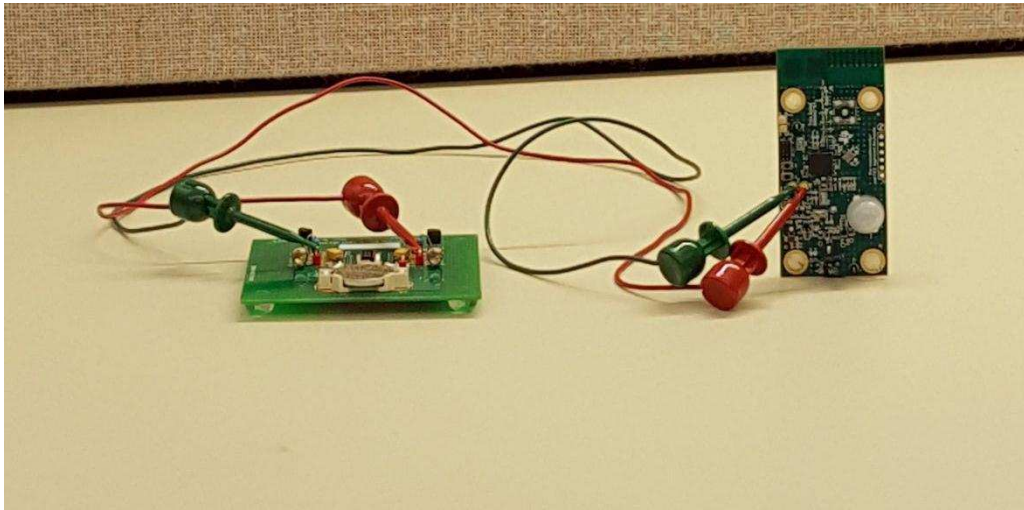


**図 21. Motion Sensitivity Test Setup  
(Top: No Motion; Bottom: Motion Detected)**

### 3.2.1.2.3 Wireless RF Range

The range of the Wireless Sub-1 GHz RF was measured using the CC1111 USB dongle. For this test, the PIR PCB remained at a stationary location as a laptop with the CC1111 USB dongle attached and listening was moved away from the PIR PCB. While the CC1111 was on the move, the PIR design was being reset at regular short intervals to make sure there were radio packets constantly being transmitted. The distance at which packets were no longer received was then measured.

Different orientations of the PCB and the CC1111 USB dongle with respect to one another were used during the test. No discernable change in the Wireless RF range was observed.

### 3.2.1.2.4 RF Immunity

The immunity of this TI Design with respect to radiated RF disturbances was measured according to IEC 61000-4-3 with an extended low frequency range. The IEC standard is specified for a frequency range of 80 MHz to 1 GHz; however, this testing was extended down to 10 kHz to look for susceptibility in the design for disturbances closer to the pass band of the circuit.

The setup consisted of connecting the pulse stretcher board used in 3.2.1.2.2 to the window comparator outputs and monitoring the LEDs for activity with a camera inside the anechoic chamber. Additionally, a field strength probe was placed near the board under test for control and monitoring of the RF field strength level being tested. This test setup is shown in 22.

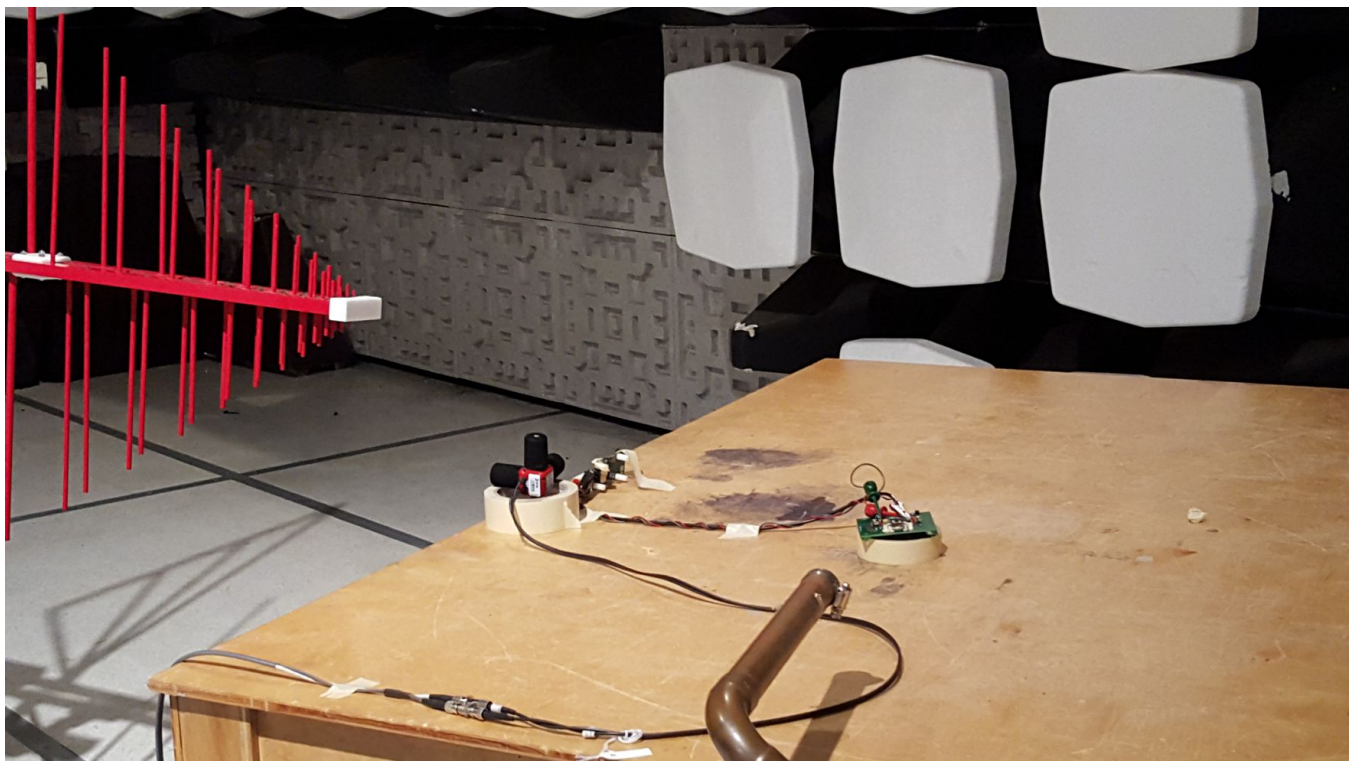


図 22. RF Immunity Test Setup

The biconical antenna shown in 22 was used for the frequency range from 30 MHz to 1 GHz in both the horizontal and vertical orientation (vertical orientation shown). For frequencies lower than 30 MHz, it was necessary to use a rod antenna in a single orientation.

### 3.2.2 Test Results

注: Unless otherwise noted, the test data in the following sections were measured with the system at room temperature. All of the measurements in this section were measured with calibrated lab equipment.

#### 3.2.2.1 Power Characterization

The supply current for the different circuit paths in this design was measured using an initial prototype design. This information was used early in the design process to balance the battery lifetime with motion sensitivity specifications and the sensor bias. This data was also compared to measurements made on the reference design hardware to make sure there was a good correlation between initial results and final results.

**表 2. Low-Power PIR Motion Detector Motion Sensitivity Results**

CIRCUIT PATH	SUPPLY CURRENT (IDLE)	
	NOMINAL	MEASURED
Sensor	600 nA	594 nA
Comparators (x2)	150 nA	150 nA
Divider	50 nA	50 nA
Opamp1	374 nA	360 nA
Opamp2	409 nA	380 nA
CC1310	100 nA	120 nA
Total	1.683 $\mu$ A	1.654 $\mu$ A

The connection events contribute to the majority of the current consumption and therefore influence battery life the most. On first power-up, the reference design must search for and join the network as discussed in 2.4.4. The connection event is approximately 49 ms long with an average current of 12.77 mA as shown in [図 23](#). This is quite a bit of current, but this only happens on initial start-up of the device or when the reference design is connected to a new network.

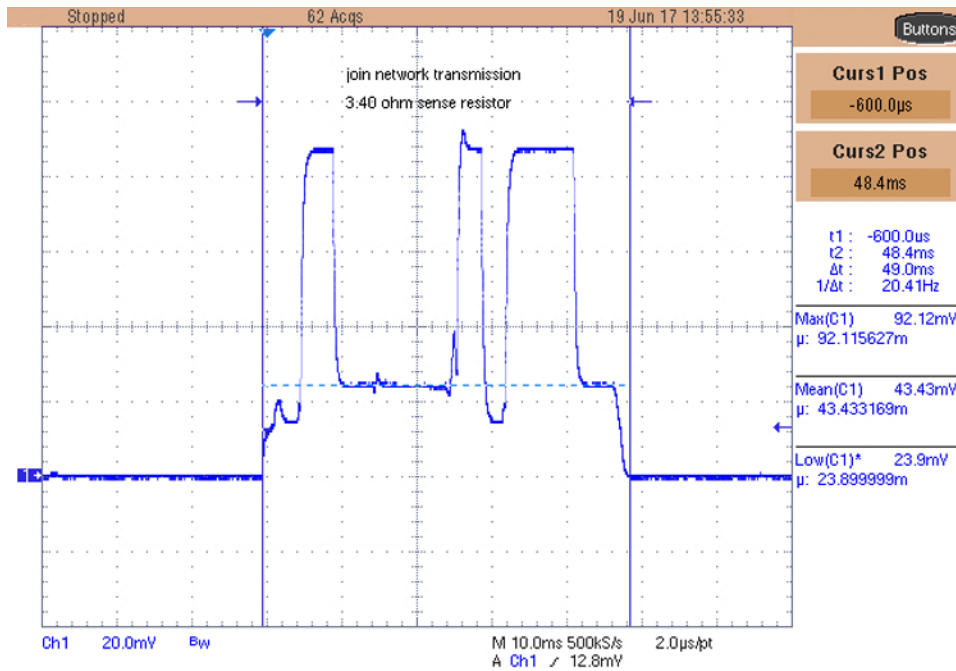


図 23. Join Sensor-to-Cloud Network Transmission

図 24 shows the packet sniffer capture of the joining network transmission. The transmission consists of a 14-byte data request packet from the sensor (0x0001), followed by an ACK from the gateway (0xaabb). The gateway sends data and the sensor node acknowledges. After that, the sensor sends the gateway its own data.

1666.381816	0x0001	0xaabb	TI 802.15.4GE	14Data request
1666.387928			TI 802.15.4GE	7Ack
1666.392069	0xaabb	0x0001	TI 802.15.4GE	42Data, Dst: 0x0001, Src: 0xaabb
1666.402686			TI 802.15.4GE	7Ack
1666.409112	0x0001	0xaabb	TI 802.15.4GE	44Data, Dst: 0xaabb, Src: 0x0001
1666.420019			TI 802.15.4GE	7Ack

図 24. Join Network Packet Sniffer Capture

The next connection event occurs when movement is first detected or when an "all clear" packet is being transmitted when motion has not been detected for a minute. The "motion detected" and "all clear" packets are identical in length. The transmission takes approximately 23.28 ms with an average current of 14 mA as shown in 図 25.

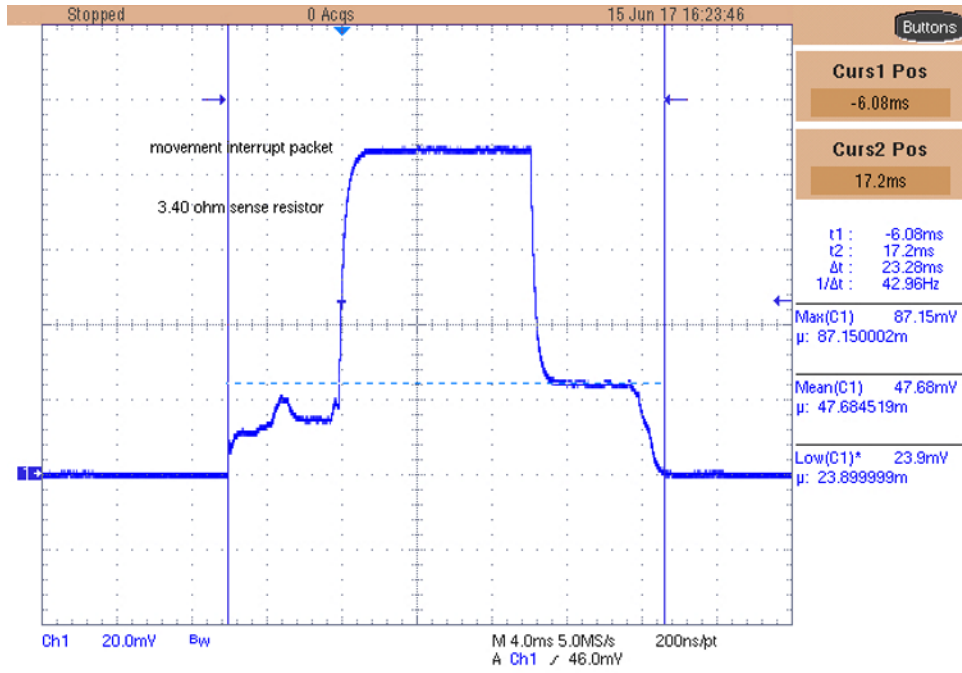
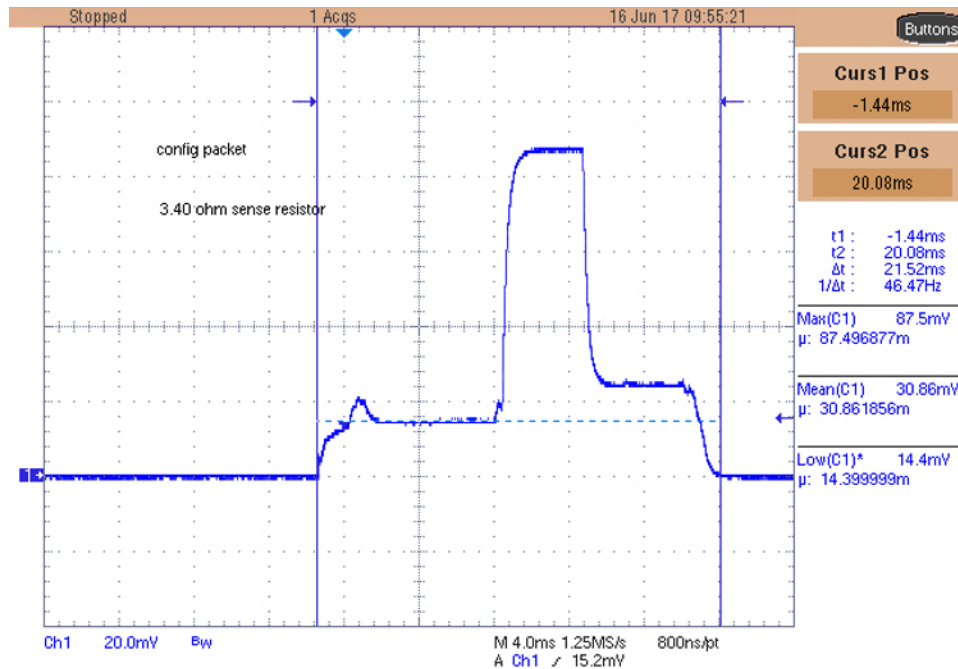


図 25. Movement Status Update on Packet Transmit

The last connection event is the configuration transmission between the gateway and the sensor node. This occurs on the Configuration Polling interval discussed in 2.4.4.  26 shows the single packet transmit and the following ACK being received. Other packets follow if there are messages from the gateway or if frequency hopping is enabled because a new frequency will be negotiated on each configuration interval. To save power frequency hopping was disabled and the configuration polling interval was set to 20 min. The configuration polling event takes approximately 21.52 ms with an average current of 9.08 mA as shown in .



 26. Configuration Packet Transmission

The data values highlighted in this section are used in the following section to calculate the expected battery life for expected use conditions.

### 3.2.2.2 Battery Life Calculations

The main parameters that affect the estimated battery life of the entire system are:

- Capacity rating of the battery in milliamp-hours (mAh)
- Average standby-state current consumption ( $\mu\text{A}$ )
- Standby-state duration (s)
- Average packet current consumption (mA)
- Packet transmission duration (ms)
- Polling rate

式 13 describes the estimated battery life of the system:

$$\text{Battery Lifetime (yr)} = \frac{\text{Battery Capacity (mAh)}}{\left( \frac{I_{\text{Standby}} (\mu\text{A}) \times t_{\text{Standby}} (\text{s}) + I_{\text{Data}} (\mu\text{A}) \times t_{\text{Data}} (\text{s}) + I_{\text{Poll}} (\mu\text{A}) \times t_{\text{Poll}} (\text{s})}{t_{\text{Total}} (\text{s})} \right)} \times \frac{1 \text{ year}}{8760 \text{ hours}} \times \text{Derating Factor} \quad (13)$$

where:

- $t_{\text{Total}}$  is an arbitrary time interval
- $t_{\text{Data}}$  is the amount of time spent transmitting data packets
- $t_{\text{Poll}}$  is the amount of time transmitting poll packets

If  $t_{\text{Total}}$  is set equal to the polling interval (30 min), then  $t_{\text{Poll}}$  equals the time it takes to send a single poll packet, 21.56 ms. The value for  $t_{\text{Data}}$  is calculated as:

$$t_{\text{Data}} = n \left( \frac{\text{Events}}{\text{hr}} \right) \times \frac{1 \text{ hr}}{3600 \text{ s}} \times t_{\text{Total}} \times t_{\text{DataPkt}} \quad (14)$$

where:

- $n$  is the number of movement event packets per hour
- $t_{\text{DataPkt}}$  is the amount of time it takes to send a movement status update data packet, 23.28 ms

The number of motion events per hour depends entirely on the end-use case. However, for the purpose of this TI Design, the following use-case was defined:

- Detector installation
- Six events per hour
- One minute active movement timer; if no movement after 1 minute of seeing motion, an "all clear" packet is sent.
- Polling interval of 30 minutes

Using these requirements, the  $t_{\text{Data}}$  can be calculated as follows:

$$t_{\text{Data}} = 6 \left( \frac{\text{Events}}{\text{hr}} \right) \times \frac{1 \text{ hr}}{3600 \text{ s}} \times 23.28 \text{ ms} \times t_{\text{Total}} \quad (15)$$

$$t_{\text{Data}} = 38.8 \times 10^{-6} \times t_{\text{Total}} = 69.84 \text{ ms}$$

Another available knob in the optimization of battery life for this reference design is the active timer value. The default value in firmware is 1 minute. Because this value can be modified, the battery life for Case 1 and Case 3 are recalculated using a value of 30 seconds to show the expected improvement.

The equations for the expected battery life for the three cases in consideration are as follows.

General lifetime equation:

$$\text{BatteryLifetime (years)} = \frac{240 \text{ mAh}}{\left( \frac{1.65 \mu\text{A} \times (1800 \text{ s}) + 14 \text{ mA} \times 69.84 \text{ ms} + 9.08 \text{ mA} \times 22 \text{ ms}}{1800 \text{ s}} \right)} \times \frac{1 \text{ year}}{8760 \text{ hrs}} \times 0.85 = 10.1 \text{ years}$$

(16)

The derating factor in these equations accounts for self aging of the battery. Based on these equations, 表 3 and 図 27 show the average expected battery lifetime for this reference design with the active timer set to 1 minute and the polling interval from 1 minute to 1 hour.

**表 3. Battery Lifetime versus Polling Interval**

T <sub>POLL</sub> (min)	T <sub>POLL</sub> (s)	I <sub>STANDBY</sub> (A)	t <sub>STANDBY</sub> (s)	I <sub>POLL</sub> (A)	t <sub>POLL</sub> (s)	I <sub>DATA</sub> (A)	t <sub>DATA</sub> (s)	I <sub>AVG</sub> (A)	BATT CAP (Ah)	DERATING	BATT LIFE (yrs)
1.0E+0	60.0E+0	1.65E-6	59.98E+0	9.08E-3	22.00E-3	14.02E-3	2.33E-3	5.52E-6	240.0E-3	0.85	4.22
2.0E+0	120.0E+0	1.65E-6	119.97E+0	9.08E-3	22.00E-3	14.02E-3	4.66E-3	3.86E-6	240.0E-3	0.85	6.04
5.0E+0	300.0E+0	1.65E-6	299.97E+0	9.08E-3	22.00E-3	14.02E-3	11.64E-3	2.86E-6	240.0E-3	0.85	8.14
10.0E+0	600.0E+0	1.65E-6	599.95E+0	9.08E-3	22.00E-3	14.02E-3	23.28E-3	2.53E-6	240.0E-3	0.85	9.22
20.0E+0	1.2E+3	1.65E-6	1.20E+3	9.08E-3	22.00E-3	14.02E-3	46.56E-3	2.36E-6	240.0E-3	0.85	9.87
21.0E+0	1.3E+3	1.65E-6	1.26E+3	9.08E-3	22.00E-3	14.02E-3	48.89E-3	2.35E-6	240.0E-3	0.85	9.90
24.0E+0	1.4E+3	1.65E-6	1.44E+3	9.08E-3	22.00E-3	14.02E-3	55.87E-3	2.33E-6	240.0E-3	0.85	9.98
27.0E+0	1.6E+3	1.65E-6	1.62E+3	9.08E-3	22.00E-3	14.02E-3	62.86E-3	2.32E-6	240.0E-3	0.85	10.05
30.0E+0	1.8E+3	1.65E-6	1.80E+3	9.08E-3	22.00E-3	14.02E-3	69.84E-3	2.30E-6	240.0E-3	0.85	10.10
33.0E+0	2.0E+3	1.65E-6	1.98E+3	9.08E-3	22.00E-3	14.02E-3	76.82E-3	2.29E-6	240.0E-3	0.85	10.15
36.0E+0	2.2E+3	1.65E-6	2.16E+3	9.08E-3	22.00E-3	14.02E-3	83.81E-3	2.29E-6	240.0E-3	0.85	10.19
39.0E+0	2.3E+3	1.65E-6	2.34E+3	9.08E-3	22.00E-3	14.02E-3	90.79E-3	2.28E-6	240.0E-3	0.85	10.22
42.0E+0	2.5E+3	1.65E-6	2.52E+3	9.08E-3	22.00E-3	14.02E-3	97.78E-3	2.27E-6	240.0E-3	0.85	10.24
45.0E+0	2.7E+3	1.65E-6	2.70E+3	9.08E-3	22.00E-3	14.02E-3	104.76E-3	2.27E-6	240.0E-3	0.85	10.27
48.0E+0	2.9E+3	1.65E-6	2.88E+3	9.08E-3	22.00E-3	14.02E-3	111.74E-3	2.26E-6	240.0E-3	0.85	10.29
51.0E+0	3.1E+3	1.65E-6	3.06E+3	9.08E-3	22.00E-3	14.02E-3	118.73E-3	2.26E-6	240.0E-3	0.85	10.31
54.0E+0	3.2E+3	1.65E-6	3.24E+3	9.08E-3	22.00E-3	14.02E-3	125.71E-3	2.26E-6	240.0E-3	0.85	10.32
57.0E+0	3.4E+3	1.65E-6	3.42E+3	9.08E-3	22.00E-3	14.02E-3	132.70E-3	2.25E-6	240.0E-3	0.85	10.34
60.0E+0	3.6E+3	1.65E-6	3.60E+3	9.08E-3	22.00E-3	14.02E-3	139.68E-3	2.25E-6	240.0E-3	0.85	10.35
64.0E+0	3.8E+3	1.65E-6	3.84E+3	9.08E-3	22.00E-3	14.02E-3	148.99E-3	2.25E-6	240.0E-3	0.85	10.37
16.7E+3	1.0E+6	1.65E-6	999.96E+3	9.08E-3	22.00E-3	14.02E-3	38.80E+0	2.19E-6	240.0E-3	0.85	10.61

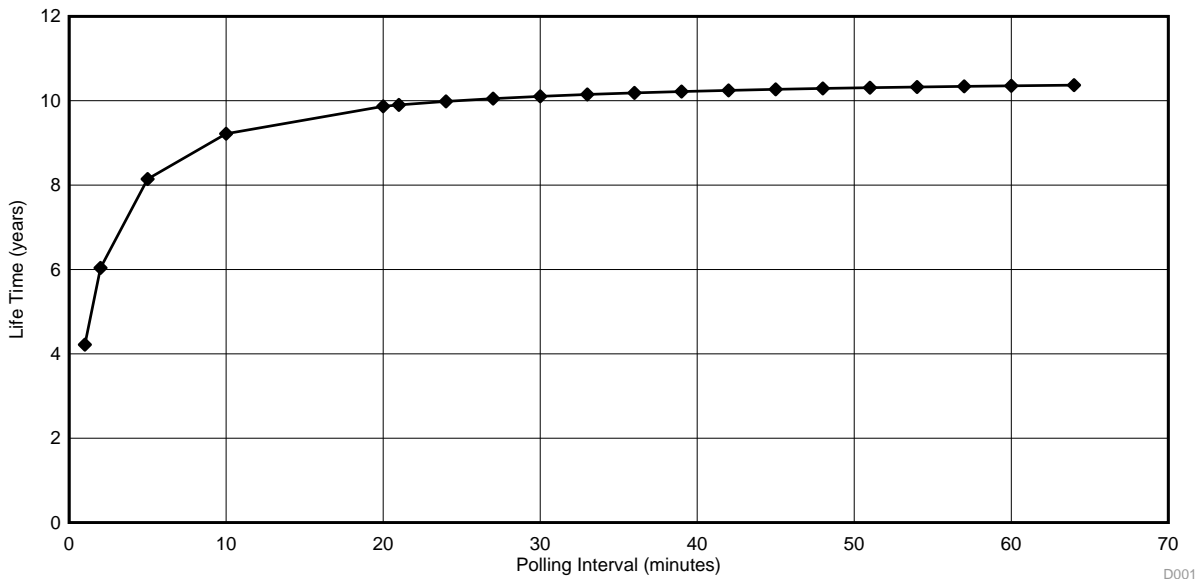


**図 27. Battery Lifetime vs Polling Interval**

### 3.2.2.3 Functional

#### 3.2.2.3.1 Motion Sensitivity

The motion sensitivity was measured for multiple sensors with different bias conditions and two different gain settings. 表 4 summarizes these measurement results.

表 4. Low-Power PIR Motion Detector Motion Sensitivity Results

SENSOR	SUPPLY CURRENT (IDLE)	V <sub>OUT</sub> (DC)	MAX. DISTANCE (Av = 90 dB)	MAX. DISTANCE (Av = 70 dB)
<b>RS = 2.2 MΩ, RD = 1 MΩ</b>				
IRS-B210ST01	365 nA	0.78 V	20 ft	6 ft
IRS-B340ST02	355 nA	0.764 V	25 ft	8 ft
IRA-E700ST0	500 nA	1.093 V	12 ft	4.5 ft
IRA-E712ST3	555 nA	1.204 V	13 ft	5 ft
<b>RS = 1.3 MΩ, RD = 620 kΩ</b>				
IRS-B210ST01	594 nA	0.77 V	> 30 ft	6.5 ft
IRS-B340ST02	572 nA	0.744 V	27 ft	8 ft
IRA-E700ST0	838 nA	1.085 V	15 ft	5 ft
IRA-E712ST3	920 nA	1.178 V	17 ft	7.5 ft

The highlighted cell in 表 4 illustrates the motion sensitivity of the circuit configuration implemented in this TI Design.

#### 3.2.2.3.2 Wireless RF Range

The wireless RF range was measured to be 220 meters in a typical office environment with partial line of sight. The measured signal strength at this distance was less than -100 dBm as measured by the CC1111 packet sniffer dongle.

While this distance is outstanding considering the small footprint of the PCB antenna, there are ways to increase this distance even further. Use of a whip antenna with gain instead of the passive PCB antenna could offer improvements in the wireless RF range. Another option would be to increase the transmit power of the CC1310 to its maximum level at the expense of increased supply current during the radio transmission intervals.

### 3.2.2.3.3 RF Immunity

The RF immunity of this design was measured to be 30 V/m over the entire 10-kHz to 1-GHz frequency range. Immunity at field strengths higher than this were not tested due to equipment limitations in the frequency range around 30 MHz. This level also corresponds to Class 3 in the IEC 61000-4-3 standard.

The only anomaly observed during this test was at the singular frequency step of 728.5 MHz, where the passing immunity level dropped to 29.8 V/m in the horizontal antenna orientation. This drop was due to the wiring connection between the PIR PCB and the pulse stretcher board used for monitoring.

### 3.2.2.3.4 Vibration

Vibration was not tested on this reference design in any official capacity. Part of the reasoning for this is that finding vibration specifications on commercially available PIR motion detectors is difficult to find. Rudimentary vibration testing was performed in the lab by beating on the desk on which the PIR was also resting and looking for false trigger events at the output of the window comparator. Based on this test, no false triggers were observed as long as the PCB did not physically move. While crude, this test does show that there is nothing systematic in the design itself that would cause false triggers in a normal application aside from the sensor construction itself.

A more informative test would include control over vibration frequency and amplitude with both of these being varied. The results of such a test would illustrate potential harmonic sensitivities to vibration. PCB orientation could also be varied as part of this test for a complete picture of the sensitivity to vibration for a given design in different installations. Because such an elaborate test would yield different results based on the physical enclosure that would finally house the PCB design, it was determined that this was beyond the scope of this reference design.

All PIR-based motion sensors are sensitive to vibration in some capacity due to the physical construction of the sensor as well as the way it naturally operates. Because the PIR sensor is built using thermopiles, these elements have a crystal structure, which exhibits a piezoelectric effect if the amplitude and frequency of vibration is such that the thermopiles themselves vibrate. A more prevalent effect is due to the entire sensor itself moving. Because a Fresnel lens enlarges the effective field of view of the sensor at substantial distances away from the sensor by focusing IR energy onto the small area of the sensor elements, any small movement of the sensor will result in large movements in the field of view. Due to background IR energy, the sensor output will not be able to distinguish between changes in IR energy due to motion with a static background or the background itself changing rapidly due to movements of the field of view.

In other words, the detection of motion is relative. If the sensor is assumed to be perfectly static, motion detected will be relative to the sensor; however, motion will also be detected if the background is static but the sensor is moving. In both cases, the output is valid because there is motion, but the task of narrowing the output to what is desired falls upon the installation and enclosure design.

## 4 Design Files

### 4.1 Schematics

To download the schematics, see the design files at [TIDA-01476](#).

### 4.2 Bill of Materials

To download the bill of materials (BOM), see the design files at [TIDA-01476](#).

### 4.3 PCB Layout Recommendations

To ensure high performance, the Low-Power Wireless PIR Motion Detector Reference Design Enabling Sensor-to-Cloud Networks TI Design was laid out using a four-layer PCB. The second layer is a solid GND pour, and the third layer is used for power rail routing with GND fills in unused areas. The top and bottom layers are used for general signal routing and also have GND fills in unused areas. For all of the TI products used in this TI Design, adhere to the layout guidelines detailed in their respective datasheets.

Additionally, because of the low-power design and the resulting high-impedance paths present in the design, keep the signal routes in the analog sensor path between the PIR sensor output and the window comparator input as short as possible with adequate GND fill around these signals.

If this design is to be used in an environment where dust or moisture accumulation is possible, be aware that it may be necessary to include a conformal coating to eliminate additional leakage paths due to the operating environment over time.

The antenna on this TI Design is the miniature helical PCB antenna for 868 MHz or 915 MHz. See the application note DN038 ([SWRA416](#)) for more details about layout and performance.



## 5 Software Files

To download the software files, see the design files at [TIDA-01476](#).

## 6 Related Documentation

1. Texas Instruments, [Sub-1 GHz Sensor to Cloud Industrial IoT Gateway Reference Design](#), TIDEP-0084 Design Guide (TIDUCI9)
2. Texas Instruments, [Reverse Current/Battery Protection Circuits](#), Application Report (SLVA139)
3. Texas Instruments, [Coin Cells and Peak Current Draw](#), WP001 White Paper (SWRA349)
4. Texas Instruments, [Miniature Helical PCB Antenna for 868 MHz or 915/920 MHz](#), DN038 Application Report (SWRA416)
5. Texas Instruments, [WEBENCH® Design Center](#) (<http://www.ti.com/webench>)
6. Texas Instruments, [Low Power Wireless PIR Motion Detector Reference Design Enabling 10 Year Coin Cell Battery Life](#), TIDA-00489 Design Guide (TIDUAU1)

### 6.1 商標

PowerWise, SmartRF, Code Composer Studio, LaunchPad, MSP430 are trademarks of Texas Instruments.

WEBENCH is a registered trademark of Texas Instruments.

ARM, Cortex, IAR Embedded Workbench are registered trademarks of ARM Ltd.

*Bluetooth* is a registered trademark of Bluetooth SIG.

ULPBench is a trademark of Embedded Microprocessor Benchmark Consortium.

CoreMark is a registered trademark of Embedded Microprocessor Benchmark Consortium.

Energizer is a registered trademark of Energizer Brands, LLC.

Windows, Microsoft, Excel are registered trademarks of Microsoft.

Murata is a registered trademark of Murata Manufacturing Co., Ltd.

Vaisala is a registered trademark of Vaisala.

Watlow is a registered trademark of Watlow Electric Manufacturing Company.

すべての商標および登録商標はそれぞれの所有者に帰属します。

## 7 About the Authors

**JARROD KREBS** is a systems designer at Texas Instruments, where he is responsible for developing reference designs in the industrial segment. Jarrod has experience with software and embedded applications implemented on ARM-based microcontrollers and TI's MSP430™ platforms. Jarrod earned his bachelor of science in computer engineering from Kansas State University in Manhattan, KS. Jarrod is also a member of the Institute of Electrical and Electronics Engineers (IEEE).

**DAVID STOUT** is a systems designer at Texas Instruments, where he is responsible for developing reference designs in the industrial segment. David has over 18 years of experience designing Analog, Mixed-Signal, and RF ICs with more than 14 years focused on products for the industrial semiconductor market. David earned his bachelor of science in electrical engineering (BSEE) degree from Louisiana State University, Baton Rouge, Louisiana and a master of science in electrical engineering (MSEE) degree from the University of Texas at Dallas, Richardson, Texas.

## TIの設計情報およびリソースに関する重要な注意事項

Texas Instruments Incorporated ("TI")の技術、アプリケーションその他設計に関する助言、サービスまたは情報は、TI製品を組み込んだアプリケーションを開発する設計者に役立つことを目的として提供するものです。これにはリファレンス設計や、評価モジュールに関する資料が含まれますが、これらに限られません。以下、これらを総称して「TIリソース」と呼びます。いかなる方法であっても、TIリソースのいずれかをダウンロード、アクセス、または使用した場合、お客様(個人、または会社を代表している場合にはお客様の会社)は、これらのリソースをここに記載された目的にのみ使用し、この注意事項の条項に従うことに合意したものとします。

TIによるTIリソースの提供は、TI製品に対する該当の発行済み保証事項または免責事項を拡張またはいかなる形でも変更するものではなく、これらのTIリソースを提供することによって、TIにはいかなる追加義務も責任も発生しないものとします。TIは、自社のTIリソースに訂正、拡張、改良、およびその他の変更を加える権利を留保します。

お客様は、自らのアプリケーションの設計において、ご自身が独自に分析、評価、判断を行う責任がお客様にあり、お客様のアプリケーション(および、お客様のアプリケーションに使用されるすべてのTI製品)の安全性、および該当するすべての規制、法、その他適用される要件への遵守を保証するすべての責任をお客様のみが負うことを理解し、合意するものとします。お客様は、自身のアプリケーションに関して、(1) 故障による危険な結果を予測し、(2) 障害とその結果を監視し、および、(3) 損害を引き起こす障害の可能性を減らし、適切な対策を行う目的で、安全策を開発し実装するために必要な、すべての技術を保持していることを表明するものとします。お客様は、TI製品を含むアプリケーションを使用または配布する前に、それらのアプリケーション、およびアプリケーションに使用されているTI製品の機能性を完全にテストすることに合意するものとします。TIは、特定のTIリソース用に発行されたドキュメントで明示的に記載されているもの以外のテストを実行していません。

お客様は、個別のTIリソースにつき、当該TIリソースに記載されているTI製品を含むアプリケーションの開発に関連する目的でのみ、使用、コピー、変更することが許可されています。明示的または黙示的を問わず、禁反言の法理その他どのような理由でも、他のTIの知的所有権に対するその他のライセンスは付与されません。また、TIまたは他のいかなる第三者のテクノロジーまたは知的所有権についても、いかなるライセンスも付与されるものではありません。付与されないものには、TI製品またはサービスが使用される組み合わせ、機械、プロセスに関連する特許権、著作権、回路配置利用権、その他の知的所有権が含まれますが、これらに限られません。第三者の製品やサービスに関する、またはそれらを参照する情報は、そのような製品またはサービスを利用するライセンスを構成するものではなく、それらに対する保証または推奨を意味するものでもありません。TIリソースを使用するため、第三者の特許または他の知的所有権に基づく第三者からのライセンス、あるいはTIの特許または他の知的所有権に基づくTIからのライセンスが必要な場合があります。

TIのリソースは、それに含まれるあらゆる欠陥も含めて、「現状のまま」提供されます。TIは、TIリソースまたはその仕様に関して、明示的か暗黙的にかかわらず、他のいかなる保証または表明も行いません。これには、正確性または完全性、権原、続発性の障害に関する保証、および商品性、特定目的への適合性、第三者の知的所有権の非侵害に対する黙示的保証が含まれますが、これらに限られません。

TIは、いかなる苦情に対しても、お客様への弁済または補償を行う義務はなく、行わないものとします。これには、任意の製品の組み合わせに関連する、またはそれらに基づく侵害の請求も含まれますが、これらに限られず、またその事実についてTIリソースまたは他の場所に記載されているか否かを問わないものとします。いかなる場合も、TIリソースまたはその使用に関連して、またはそれらにより発生した、実際の、直接的、特別、付随的、間接的、懲罰的、偶発的、または、結果的な損害について、そのような損害の可能性についてTIが知らされていたかどうかにかかわらず、TIは責任を負わないものとします。

お客様は、この注意事項の条件および条項に従わなかったために発生した、いかなる損害、コスト、損失、責任からも、TIおよびその代表者を完全に免責するものとします。

この注意事項はTIリソースに適用されます。特定の種類の資料、TI製品、およびサービスの使用および購入については、追加条項が適用されます。これには、半導体製品(<http://www.ti.com/sc/docs/stdterms.htm>)、評価モジュール、およびサンプル(<http://www.ti.com/sc/docs/sampterm.htm>)についてのTIの標準条項が含まれますが、これらに限られません。